https://doi.org/10.5194/egusphere-2025-1311
Preprint. Discussion started: 31 March 2025

ENSO-Driven Variability of Deep Ocean Circulation in the Southeast Pacific

Manuel Torres-Godoy[1,2], Oscar Pizarro[2,3], Boris Dewitte[4,5,6], Vera Oerder[2,7]

[1]Programa de Postgrado en Oceanografía, Universidad de Concepción, Concepción, Chile
[2]Instituto Milenio de Oceanografía, Concepción, Chile
[3]Departamento de Geofísica, Universidad de Concepción, Concepción, Chile
[4]Centro de Estudios Avanzados en Zonas Áridas (CEAZA), La Serena, Chile.
[5]Center for Ecology and Sustainable Management of Oceanic Islands (ESMOI), Departamento de Biología Marina, Universidad Católica del Norte, Chile.
[6]CECI, Université de Toulouse III, CERFACS/CNRS, Toulouse, France.
[7]Departamento de Oceanografía, Universidad de Concepción, Concepción, Chile

Correspondence to: Oscar Pizarro (oscar.pizarro@imo-chile.cl)

Abstract. The Southeast Pacific is crucial for transporting Pacific Deep Water toward the Southern Ocean, primarily through a persistent deep southward flow off the Chilean coast. However, the variability and underlying dynamics of this flow remain poorly understood. Here, we investigate its interannual variability and explore its relationship with El Niño–Southern Oscillation (ENSO). Using the GLORYS12 global ocean reanalysis (1993–2020) and repeated GO-SHIP/WOCE P06 hydrographic sections, we focus on the 2200–4000 m depth range, covering the steep continental slope and the Atacama Trench region. Our analysis confirms a robust southward transport of approximately 2.5 Sv within ~300 km from the coast, predominantly concentrated within 100 km of the continental margin. ENSO exerts a significant influence on this current, with an intensification of the deep southward flow during El Niño events and a weakening during La Niña. This modulation is linked to large-scale oceanic adjustments, including the westward propagation of extratropical Rossby waves, which transfer energy from the surface and thermocline to the deep ocean along steep ray paths consistent with linear theory. Complex Empirical Orthogonal Function (CEOF) analysis and dynamical mode decomposition further reveals that high order baroclinic modes play a key role in shaping deep current variability. Mesoscale processes also seem to contribute to the observed variability. Enhanced deep eddy kinetic energy (EKE) occurs near the continental margin and in the coastal transition zone, which is more prominent during ENSO events. The Analysis of Reynolds stresses and vertical buoyancy fluxes (VBF) indicates that energy is transferred between mean flow and turbulence, with VBF being a dominant contributor to deep variability of EKE tendency. These findings emphasize the complex interplay of large-scale climatic forcing, topography, and mesoscale turbulence in shaping deep ocean circulation. Future work should integrate sustained deep-ocean observations and high-resolution modelling to refine our understanding of the DESPC and its role in the Pacific Meridional Overturning Circulation.

https://doi.org/10.5194/egusphere-2025-1311
Preprint. Discussion started: 31 March 2025

1 Introduction

A deep southward flow in the Southeast Pacific, off the coast of Chile, has been widely recognized through hydrographic data and geostrophic calculations (e.g., Reid, 1973; Warren, 1973; Tsimplis et al., 1998; Wijffels et al., 2001; Shaffer et al., 2004; Hernandéz-Guerra & Talley, 2016; Schulze & Speer, 2019; Arumí-Planas et al., 2022). This flow transports Pacific Deep Water to the Southern Ocean and is a fundamental component of the Meridional Overturning Circulation (MOC) (Broecker, 1991). Due to the absence of deep-water mass formation in the North Pacific, some authors describe the Pacific branch of the MOC as weaker or or less vigorous compared to the Atlantic Meridional Overturning Circulation (e.g. Burls et al., 2017; Curtis & Fedorov, 2024; Holbourn et al., 2024). For this reason, the dynamics of deep Pacific circulation and its southward flow have received considerably less attention compared to other deep currents. Both realistic and idealized models have shown that this flow is controlled by a complex interplay of topography, stratification, and large-scale oceanographic processes. The potential vorticity balance of the current is dominated by the advection of planetary vorticity and vortex stretching, where the latter is driven by the eddy temperature transport (Yang et al., 2020a, 2021).

The deep ocean off central Chile is characterized by a complex interplay of water masses that influence its circulation, stratification, and biogeochemical properties (Shaffer et al., 2004; Silva et al., 2009; Reyes-Macaya et al., 2022). The dominant deep-water mass in the region is Pacific Deep Water (PDW), which originates primarily from the North Pacific and is modified as it flows southward. PDW is distinguished by its relatively low salinity (compared to the Atlantic Deep Water) and high nutrient content, forming a significant portion of the deep ocean volume in the South Pacific (Kawabe & Fujio, 2010). Overlying and interacting with PDW is Circumpolar Deep Water (CDW), which enters the region from the Antarctic Circumpolar Current. CDW is often subdivided into Upper Circumpolar Deep Water (UCDW), which is relatively warmer and more oxygen-poor, and Lower Circumpolar Deep Water (LCDW), which is colder and denser. Both UCDW and LCDW are nutrient-rich, contributing to the region's biogeochemical cycling. At intermediate depths, Antarctic Intermediate Water (AAIW), formed in the Southern Ocean, plays a critical role in the water-mass structure (Li et al., 2022). Although AAIW is typically centred above 1000 m, it can mix downward, influencing the properties of deeper layers. These water masses collectively shape the hydrographic and dynamical characteristics of the region, driving the deep southward flow and modulating its variability in response to large-scale climate forcing.

The first direct current observations, based on several years of current-meter data between about 1300 m and 3800 m depth off the Chilean coast near 30°S, confirmed the presence of a persistent deep southward flow (Shaffer et al., 2004). In this work, the authors combined direct current measurements with hydrographic data from the WOCE P06E transect carried out in 1992 to estimate the meridional transport at 32°30'S. Below approximately 1200 m depth, they estimated a southward transport of about 10 Sv between the Chilean coast and 1500 km offshore. Subsequent studies, using different repetitions of the P06E line, have confirmed the presence of this Deep Southeast Pacific Current (DSPC) flowing southward in the Chile Basin (Schulze & Speer, 2019; Arumí-Planas et al., 2022). Different studies have emphasized the role of bottom topography in the dynamics of the deep flow (Schulze & Speer, 2019; Yang et al., 2020a, 2021) and have localized the core of the deep current over the Atacama trench (also named Peru-Chile trench). Based on hydrographic observations, Kawabe and Fujio (2010) provide a comprehensive synthesis of Pacific circulation, analysing the pathways of Lower Circumpolar Deep Water (LCDW) as it moves through the Pacific Ocean. They identify a deep flow in the eastern South Pacific that transports approximately 13 Sv of modified PDW southward, forming part of a larger, basin-scale, circulation system connecting the Pacific basin with the Southern Ocean. Previous studies have also recognized that this deep southward flow is connected to the basin scale circulation (e.g., Reid, 1973; Warren, 1973; Leth et al., 2004; Shaffer et al., 2004) and form part of the outflow branch of the Pacific meridional overturning circulation.

Although a significant portion of the South Pacific outflow likely occurs within the Chile Basin, the dynamics and low-frequency variability of the DSPC remain poorly understood. The El Niño-Southern Oscillation (ENSO), a primary driver of interannual variability in the Southeast Pacific, plays a crucial role in sea surface temperature, thermocline depth, sea level, and coastal current variability (e.g., Montecinos et al., 2005; Shaffer et al., 1999; Pizarro et al., 2001; Dewitte et al. 2008). However, its impacts on the deep ocean remain scarcely studied. Near the coast, current variability is mainly modulated by coastal-trapped waves, which influence sea level height, thermocline depth, and coastal currents. At low-frequency (periods of several months or longer) near-shore fluctuations can propagate offshore and vertically as extratropical Rossby waves (e.g., Pizarro et al., 2001; Vega et al., 2003; Dewitte et al. 2008; Dewitte et al., 2021; Arumí-Planas et al., 2022), transmitting interannual variability throughout the water column, from the thermocline to the deep ocean (Ramos et al., 2008; Vergara et al., 2017). Consequently, ENSO cycles may have a direct impact on deep ocean variability in the eastern South Pacific, modulating the characteristics of the southward deep ocean flow observed off Chile.

Eastern ocean boundaries also present large mesoscale activity in the form of mesoscale surface and subsurface eddies (Hormazabal et al., 2004; Chaigneau et al., 2008; Contreras et al., 2019). Thes eddies can induce significant intraseasonal (30-120 days) variability in flow patterns, affecting the distribution of tracers and momentum, and potentially altering the mean transport pathways of deep-water masses. Yang et al. (2020a) showed that mesoscale eddies can lead to transient reversals in the deep flow direction, obscuring the interpretation of current observations and requiring careful analysis of both observational data and model outputs. Furthermore, nonlinear interactions of mesoscale eddies may result in a net transfer of momentum, generating a net mean current (Hogg et al., 2009; Rhines & Holland, 1979). Although recent studies have addressed mesoscale eddy rectification in subsurface eastern boundary current formation (e.g., Stewart et al., 2024), the impact of this rectification process on the DSPC off the coast of Chile remains practically unknown.

Here, we examine the variability of the deep southward flow in the Chile Basin and its relationship with El Niño cycles using GLORYS12 ocean reanalysis. Our findings indicate that Rossby waves and mesoscale processes play a crucial role in shaping the DESPC and its low-frequency variability. During El Niño periods, this current intensifies, with extratropical Rossby waves modulating meridional velocity anomalies and transferring energy to the deep flow. Additionally, mesoscale

https://doi.org/10.5194/egusphere-2025-1311
Preprint. Discussion started: 31 March 2025

features contribute to the transfer of mean kinetic energy to eddy kinetic energy (EKE), particularly during El Niño. Vertical buoyancy fluxes (VBF) near the continental margin and Atacama Trench further enhance EKE, highlighting the dynamic interactions that drive deep ocean variability in the region.

The remainder of this paper is structured as follows: Section 2 provides a detailed description of the GLORYS reanalysis, hydrographic data, and the methodologies used to examine deep variability in the Eastern South Pacific (ESP). Section 3 presents the main results, divided into three subsections: the deep circulation off Chile (Section 3.1), the influence of El Niño cycles and low-frequency variability (Section 3.2), and the role of deep eddy kinetic energy and Reynolds stresses (Section 3.3). Section 4 contextualizes our findings, while also discussing the dynamics governing large-scale circulation and mesoscale processes. Finally, Section 5 summarizes the key findings and outlines potential directions for future research on deep ocean circulation in the eastern South Pacific.

2 Materials and Methods

2.1 Study Area

The Southeast Pacific (SP) is bounded by three major ridge systems: the Nazca Ridge in the north (around 25°S), the Chile Rise in the south (near 45°S), and the East Pacific Rise in the west (close to 110°W). A defining topographic feature is the Atacama Trench, which extends from the equatorial Pacific to roughly 36°S along the South American margin (Fig. 1). This trench has an average depth of approximately 6500 m, with maximum depths exceeding 8000 m off northern Chile (near 23°S). In the present study, we focus on the segment of the Chilean coast between ~30°S and 38°S, where steep continental margins and the adjoining trench can significantly influence deep circulation.

2.2 The GLORYS Ocean Reanalysis

To examine the variability and temporal evolution of the DSPC, we used the Global Ocean Reanalysis and Simulations version 12 (GLORYS12) dataset (Lellouche et al., 2021). GLORYS12 is based on the Nucleus for European Modeling of the Ocean (NEMO) model, forced by the ERA-Interim atmospheric reanalysis. It assimilates both satellite and in situ observations from the Coriolis Ocean database Reanalysis (CORA) over the 1993 – 2020 period. The product provides daily fields of temperature, salinity, horizontal velocity, and sea-surface height, at a horizontal resolution of approximately 1/12° (~8 km) and with 50 vertical levels extending from the surface down to ~5700 m depth. The spacing increases with depth, with 22 levels within the top 100 m, 13 levels between 100 and 1000 m and the following levels in the deep ocean: 1062, 1245, 1452, 1684, 1941, 2225, 2533, 2865, 3220, 3597, 3992, 4405, 4833, 5274, and 5727 m. This relatively high spatial and temporal resolution makes GLORYS12 particularly suited to capturing the mesoscale features characteristic and deep ocean variability in the SEP region.

Because previous studies and our preliminary results suggest that the southward flow becomes more pronounced below 2000 m in this region, our analysis focuses on depths from roughly 2000 m to 4000 m (Fig. 1). This range corresponds to six depth levels in the GLORYS12 reanalysis (2225.1 m, 2533.3 m, 2865.7 m, 3220.8 m, 3597.0 m, and 3992.5 m). We frequently average or integrate various metrics (e.g., meridional velocity, eddy kinetic energy, Reynolds stresses, buoyancy fluxes) across these levels to represent the DESPC. In some calculations, we further integrate the flow from the continental slope to a specified offshore distance, as indicated in the respective results sections. This approach ensures that we capture both the influence of the steep topography and the large-scale circulation patterns that shape the deep ocean currents in the ESP.

2.3 Hydrographic Data

To calculate observed transport in the study region we utilized the four repetitions of the WOCE P06 hydrographic sections centered at 32.5°S. This section was repeated in the years 1992, 2003, 2010, and 2017. We used temperature, salinity, and pressure data to calculate geostrophic velocities on neutral density (γn) (Jackett & McDougall, 1997; Klocker & McDougall, 2010). The no-motion reference level was defined by minimizing the variability of deep transport between transects. For this calculation we consider the transport east of 89°W and the continental slope, and below the γn = 27.52 kg/m3 neutral surface (near 1000 m depth) and above the different neutral surfaces used as reference level (using an interval of 0.01 kg/m3. Using this methodology the surface γn = 28.046 kg/m3 exhibited the smallest standard deviation (0.68 Sv) across the four repetitions. This reference level is similar to the one used by Arumí-Planas et al. (2022) and Shaffer el al. (2004) of γn = 28.1 kg/m3 and σ4 = 45.83 kg/m3 (close to 3700 m), respectively.
In accordance with the methodology proposed by Shaffer et al. (2004), the density boundaries were selected based on the characteristics of the water masses present in the region and the zonal density structures at depth. Volume transports were calculated in different portions of the section bounded by longitudes 112°W, 102°W, 89°W, 77°W, and the neutral surfaces 27.05, 27.52, 27.93, and 28.046 kg/m3 (Fig. 2). The same procedure was applied to the GLORYS12 data, which were vertically, linearly, interpolated to have a 5 m resolution. We used meridional velocity from the reanalysis instead of a geostrophic velocity estimate in order to be consistent with transports shown in Fig. 1e, f, g.
Finally, we compared the observed transports between the different GO-SHIP hydrographic sections and GLORYS using different boxes defined by the neutral density ranges.

https://doi.org/10.5194/egusphere-2025-1311
Preprint. Discussion started: 31 March 2025

2.4 Eddy Kinetic Energy and Reynold Stresses

In this study, EKE and Reynolds stresses are attributed primarily to "turbulent" fluctuations on intraseasonal timescales (ranging from about 20 days to about 90 days), which are frequently associated with mesoscale eddies in the region and with coastally trapped waves near the continental margin. We began by calculating anomaly time series (SA) from the original daily series (S) by removing their respective seasonal cycle (SSC), i.e., $SA = S - SSC$. SSC was computed using a daily average for the whole period and then applying a 31-day moving mean.

To extract interannual anomalies, we applied a 19 month Hamming filter to SA.

$$S_{IA} = Hamming(SA, 19\ months)$$

Next, we applied a 25 day Hamming filter to daily SA in order to remove high frequency (synoptic) variability from the daily anomaly time series.

The low frequency component (SA_{LF}), containing only periods longer than about 90 days, was obtained by applying a 101-day hamming filter to the daily anomaly time series

$$SA_{LF} = Hamming(SA, 101\ days)$$

Finally, the intraseasonal time series (S'_{IS}) was calculated removing the low frequency series to $SA_{25\ days}$.

$$S'_{IS} = SA_{25\ days} - SA_{LF}$$

We use these S'_{IS} time series to evaluate EKE, and the turbulent-correlation terms. In the following we use ()' to denote the intraseasonal time series. We also evaluate those terms associated with synoptic timescales (1 to 25 days); in all cases, these values were at least two orders of magnitude smaller than the corresponding intraseasonal variability. We used 25 and 101 days as our filter threshold when defining the intraseasonal period because the energy spectrum has a nearly constant slope in that range (Fig. A1).

In standard oceanographic contexts the EKE is defined as the horizontal kinetic energy per unit mass, EKE = $(u'^2+v'^2)/2$, where u' and v' represent the intraseasonal time series of zonal and meridional velocity components, respectively.

To identify potential sources and sinks in the EKE budget, we use the equation for the evolution of EKE over time (e.g., Harrison & Robinson, 1978; Cushman-Roisin & Beckers, 2011)

$$\frac{D(\mathrm{EKE})}{Dt} = \nabla \cdot F_{\mathrm{EKE}} + P + B + D$$

https://doi.org/10.5194/egusphere-2025-1311
Preprint. Discussion started: 31 March 2025

Far from the surface and other boundaries the terms most relevant are typically related to shear production by the mean flow (P) and buoyant production by eddies (B). While D is the viscous dissipation and ∇·F_EKE represents the spatial redistribution of EKE not contributing to production or dissipation (and becomes zero after integrating over the entire domain). Here P = HRS+VRS is the addition of EKE by the horizontal Reynolds stresses (HRS) and the vertical Reynolds stresses (VRS), and B is the vertical buoyant flow (VBF). In vector notation, they take the following form

$$HRS = -\overline{u'^2}\frac{\partial u}{\partial x} - \overline{u'v'}\frac{\partial u}{\partial y} - \overline{v'^2}\frac{\partial v}{\partial v} - \overline{u'v'}\frac{\partial v}{\partial x},$$

$$VRS = -\overline{u'w'}\frac{\partial u}{\partial z} - \overline{v'w'}\frac{\partial v}{\partial z},$$

$$VBF = \overline{w'b'}\ .$$

Note that EKE, HRS, VRS and VBF, are all used here per unit of mass. The vertical velocity was estimated by vertically integrating the horizontal velocity divergence between neighbor vertical grids. The HRS describes how horizontal turbulence redistributes momentum across different scales, whereas VRS governs how vertical mixing transfers horizontal momentum through the water column. The VBFs arise from the turbulent transport of buoyancy, and they are fundamental in driving vertical mixing and eddy available potential and kinetic energy exchange. We integrated HRS, VRS and VBF between 2000 - 4000 m depth using GLORYS12 default vertical levels to study the behavior in the depth range where DESPC is observed. We averaged these different terms during El Niño and La Niña periods, to evaluate the effects of ENSO on their variability.

2.4 Signal Propagation

The variability and propagation patterns along 32°S were analyzed using the low-frequency anomalies of meridional velocity. To achieve this, a Complex Empirical Orthogonal Function (CEOF) analysis was employed. CEOF enables the decomposition of the time-space variability of a field into distinct modes that are orthogonal to each other (i.e., uncorrelated), effectively isolating the primary components present in the study region. Unlike the traditional EOF method, CEOF facilitates the analysis of the propagation of dominant features within a field, which is particularly relevant here given the role of the Rossby waves radiating from the coast. By introducing a complex term (i.e., a signal in quadrature) to the original variable, the CEOF method generates an additional principal component that captures the phase, thereby allowing for the analysis of the spatial and temporal propagation associated with each mode. Since the original time series from GLORYS are not evenly spaced in the vertical –having significantly higher resolution in the upper ocean– we interpolated the time series at 5 m intervals prior to the CEOF analysis to ensure a proper representation of the eigenvectors.

https://doi.org/10.5194/egusphere-2025-1311
Preprint. Discussion started: 31 March 2025

2.5 ENSO Index and the Coastal Forcing of Rossby Waves

To differentiate between El Niño and La Niña periods, we used the Multivariate ENSO Index (MEI). The MEI is calculated as the first principal component of the combined EOF of six atmospheric and oceanographic variables over the tropical Pacific (30°S-30°N and 100°E-70°W): sea level pressure, surface wind (zonal and meridional components), sea surface temperature, air temperature, and total cloudiness (Wolter and Timlin, 1998). The El Niño periods are defined when the index is greater than +0.5 (moderated) or +1 (strong) for at least several overlapping three-month periods (typically 5 or more). Conversely, when the MEI is negative and below the thresholds (e.g., less than -0.5 or -1.0), it indicates La Niña conditions.

Alongshore disturbances of the thermocline and currents related to ENSO cycles may generate Rossby Wave in the Southeast Pacific. To quantify near coastal disturbances that originate these waves, we use the alongshore current averaged between 250-450m and the first 30 km from shore. Here, we call this time series *subsurface alongshore coastal velocity* and is denoted by V_c. Note that the well-defined poleward flow (the Peru-Chile Undercurrent) can be diagnosed by this depth range near the continental slope in this simulation (Lindford et al., 2023).

3. Results

3.1 The deep southward flow in the Chile basin

Our results, based on the GLORYS ocean reanalysis for the period 1993 – 2020, show a predominantly southward deep flow (between about 2000 and 4000 m depth) in the eastern South Pacific off Chile with greater magnitude near the continental margin (Fig. 1). The mean meridional transport of this flow between the continental margin and ~300 km offshore was of -2.52 +/- 0.59 Sv and is larger and better defined near the continental margin where about 60% of the mentioned transport takes place (-1.49 +/- 0.26 Sv in the first 100 km closest to the continental margin). This deep flow showed significant interannual variability, with slightly higher transport magnitudes during El Niño (-1.87 +/- 0.35 Sv) compared to La Niña (-1.27 +/- 0.23 Sv) (Fig. 1e, f, g). El Niño and La Niña periods were identified based on the MEI, the selection criteria and more detailed analysis of changes associated with El Niño cycles are presented in Section 3.2.

https://doi.org/10.5194/egusphere-2025-1311
Preprint. Discussion started: 31 March 2025

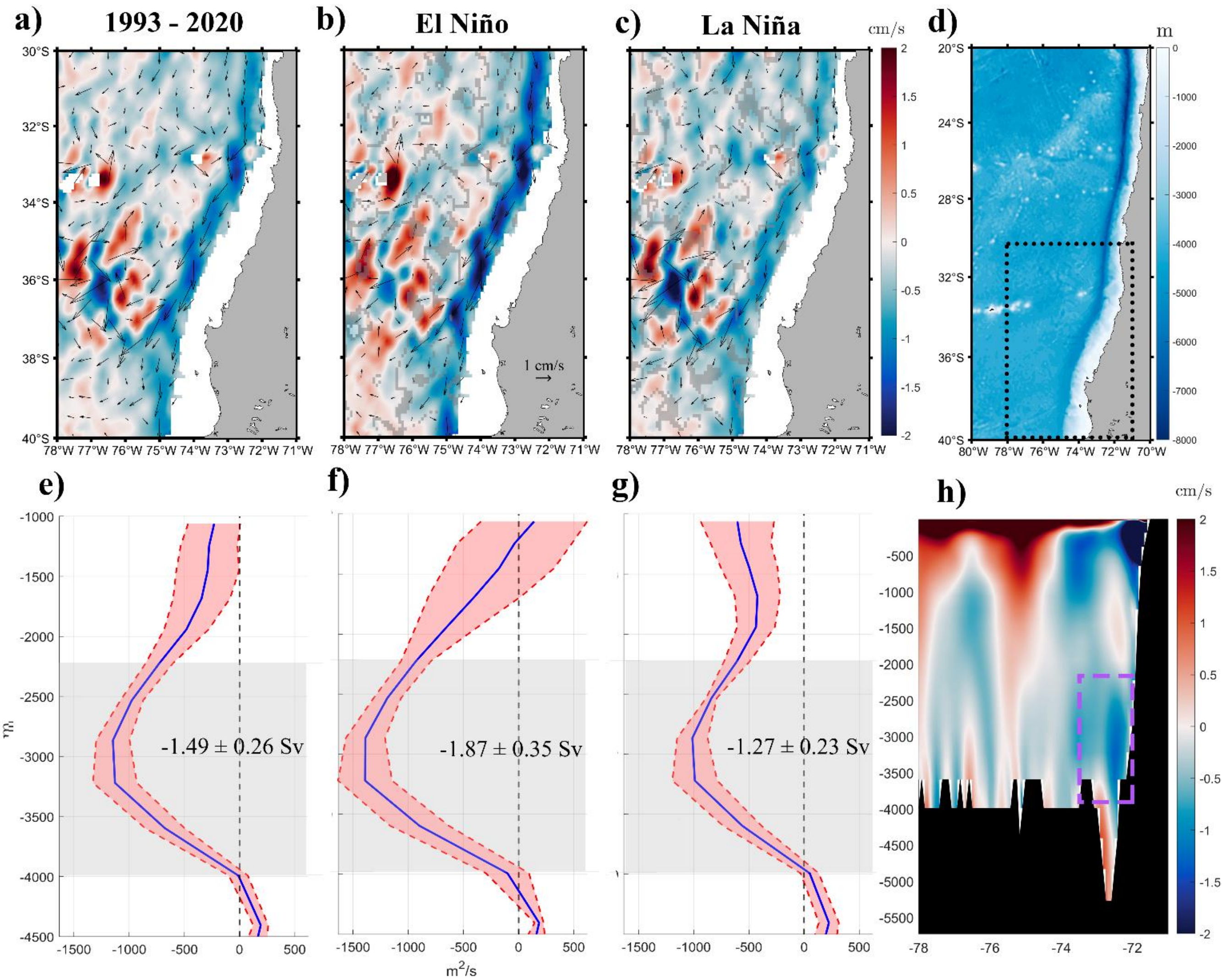

Figure 1.- Meridional velocity in the eastern South Pacific off Chile, averaged between 2225 and 3992 m depth (given the GLORYS12 vertical resolution involve specifically values at 2225, 2533, 2865, 3220, 3597, 3992 m depth): (a) for the entire study period (1993–2020), (b) during El Niño, and (c) during La Niña periods. The lower panels show the zonally integrated meridional velocity from the continental margin to 1° offshore and averaged between 30°-40°S and over (e) the entire study period (1993–2020), (f) El Niño periods, and (g) La Niña periods. Transports are in Sverdrups. The number in (e), (f) and (g) represent the mean transport between 2225 and 3992 m depth. The bathymetry of the study region is shown in (d). The dashed square highlights the region corresponding to panels (a), (b), and (c). The average flow across 32°S is shown in (h) where the dashed square in this panel is used to calculate velocity in Fig. 3.

https://doi.org/10.5194/egusphere-2025-1311
Preprint. Discussion started: 31 March 2025

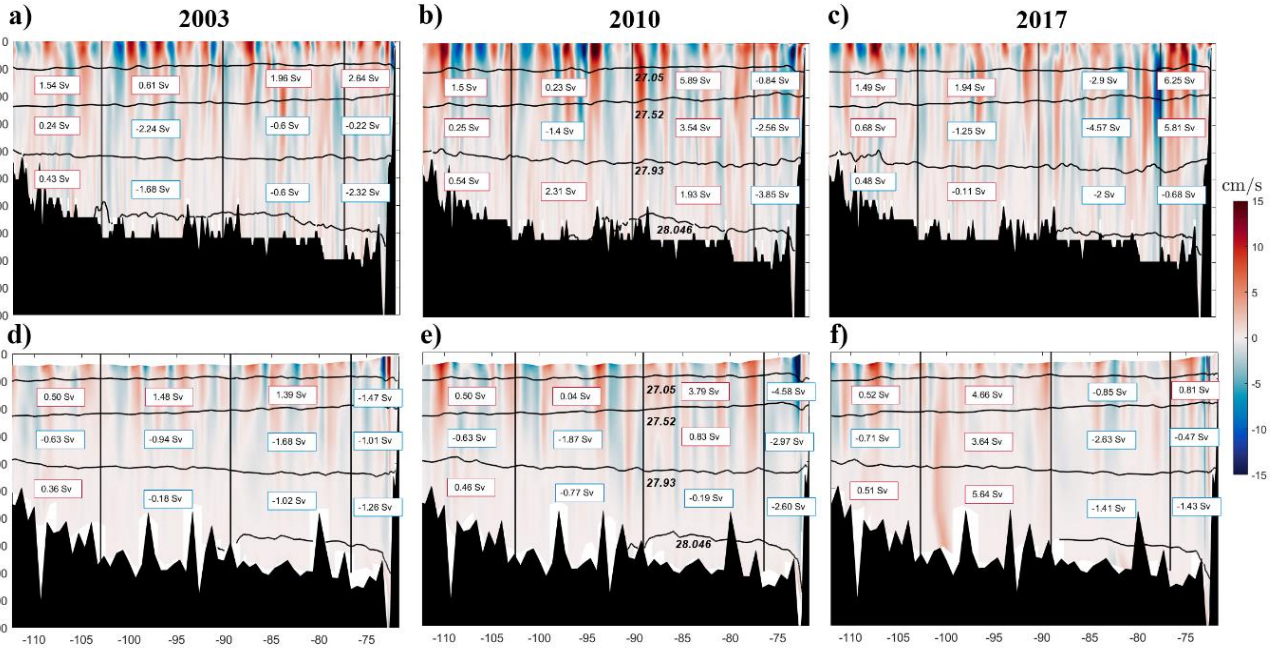

Figure 2.- Meridional velocity sections for the P06 transect in the eastern Pacific, centered at 32.5°S, for (a) 2003, (b) 2010, and (c) 2017. The upper panels show velocity from GLORYS, while the lower panels present geostrophic velocity calculated using GO-SHIP P06 hydrographic data for the same years. The GLORYS velocities were averaged over the same period as the corresponding GO-SHIP sections. Neutral density surfaces 27.050, 27.520, 27.930, and 28.046 are shown as black contours. These densities layers correspond approximately to those used by Shaffer et al. (2004) and were chosen based on the water mass properties of the region. Transport estimated between these neutral density surfaces and the longitudes indicated by the vertical black lines are shown.

The mean transport in the 4 boxes located between γ_n = 27.520 and γ_n = 28.046 (approximately between 1000 and 3500 m depth) and west of 90°W based on the 3 repetitions (Fig. 2) was -1.32 ± 1.1 Sv for the observed GO-SHIP sections, while the mean value based on GLORYS was -1.09 ± 2.37 Sv, after removing the large positive transport in the coastal box located between 27.52 and 27.93 in the 2017 section, which is associated to a large mesoscale eddy in the GLORYS reanalysis. Note that this eddy is also observed in the GO-SHIP section, but its amplitude is much smaller. In general, mesoscale eddies introduce large variability in currents in both the GLORYS reanalysis and the estimated geostrophic currents, impacting even deep ocean flow. When examining the full 1993–2020 period from GLORYS, the deep transport remains consistently southward across all coastal boxes (not shown), aligning with the mean deep transport depicted in Figure 1 and previous observational estimates (Shaffer et al., 2004; Schulze & Speer, 2019; Arumí-Planas et al., 2022). Therefore, the GLORYS reanalysis provides a reasonable representation of the deep southward flow in the eastern South Pacific off central Chile. To

https://doi.org/10.5194/egusphere-2025-1311
Preprint. Discussion started: 31 March 2025

the east of 90°W and below γ_n = 27.52 (below about 1000 m depth) transports are also predominantly southward in both the GO-SHIP and GLORYS sections, except in the 2017 GO-SHIP repetition, where large northward transport was observed between 103°W and 90°W.

3.2 Changes related to El Niño cycles and low frequency variability

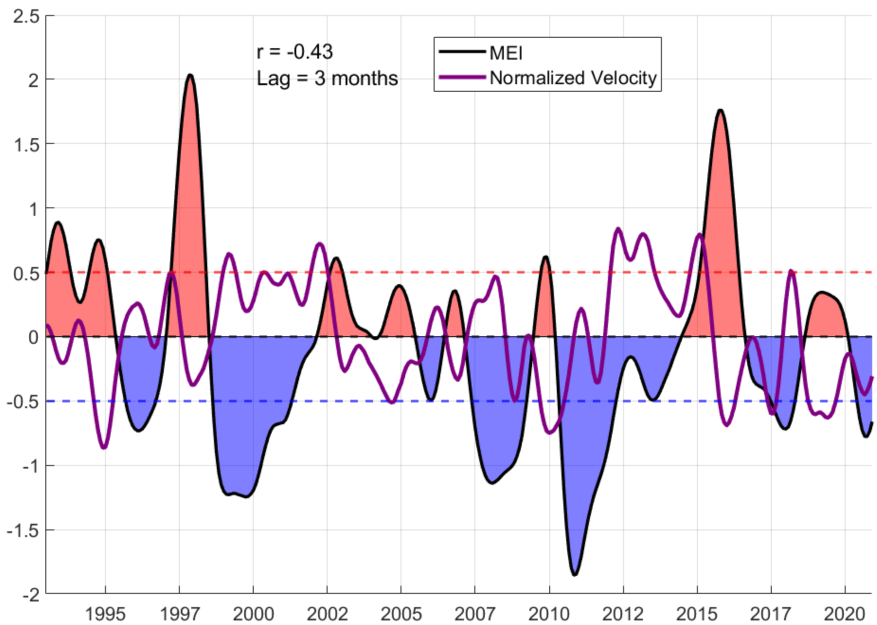

Figure 3. Multivariate El Niño Index (MEI) and normalized meridional velocity along 32°S averaged between 2225 m and 3995 m and 72° - 73.75°W as shown in Fig. 1 (h). r corresponds to the correlation between MEI and the normalized meridional velocity. MEI precedes the velocity for lagged correlation.

To examine patterns in the changes of the deep current associated with ENSO we perform a composite analysis by selecting different periods by averaging the current over multiple occurrences of El Niño, La Niña and neutral periods based on the Multivariate El Niño Index (MEI) (Figure 3). Periods with values of MEI larger (smaller) than 0.5 (-0.5) were identified as El Niño (La Niña), while periods with -0.5 < MEI < 0.5 were considered neutral. Main El Niño (red shadows) and La Niña (blue shadows) events can be clearly recognized in the MEI time series. Figure 3 also shows the alongshore velocity time-series averaged between 2225 m and 3992 m depth east of -73.75°W (rectangle in Fig. 1h). For a better comparison with the MEI, the low-frequency velocity anomalies time-series was normalized by dividing it by its standard deviation. An inverse relationship between the meridional current and the MEI can be visually recognized (the maximum correlation was r = -0.43 for a 4 moth-lag; r was significantly at 95% confidence level).

The composite analysis allows to extract common features and generate a representation of typical anomalies during those events. Fig. 4 shows the meridional current at different latitudes between 30°S and 36°S during El Niño, La Niña and neutral periods. During El Niño phases, the meridional current shows enhanced southward (blue-shaded) anomalies near the continental margin at depths below about 1500 m across all latitudes. This pattern suggests that large-scale, low-frequency adjustments in the circulation –triggered by remote equatorial forcing– can strengthen the deep southward flow along the slope. In contrast, La Niña phases typically show opposite flow anomalies, indicating a reduction or reversal of the deep southward component. Meanwhile, neutral conditions exhibit much weaker anomalies, reflecting more subdued remote forcing.

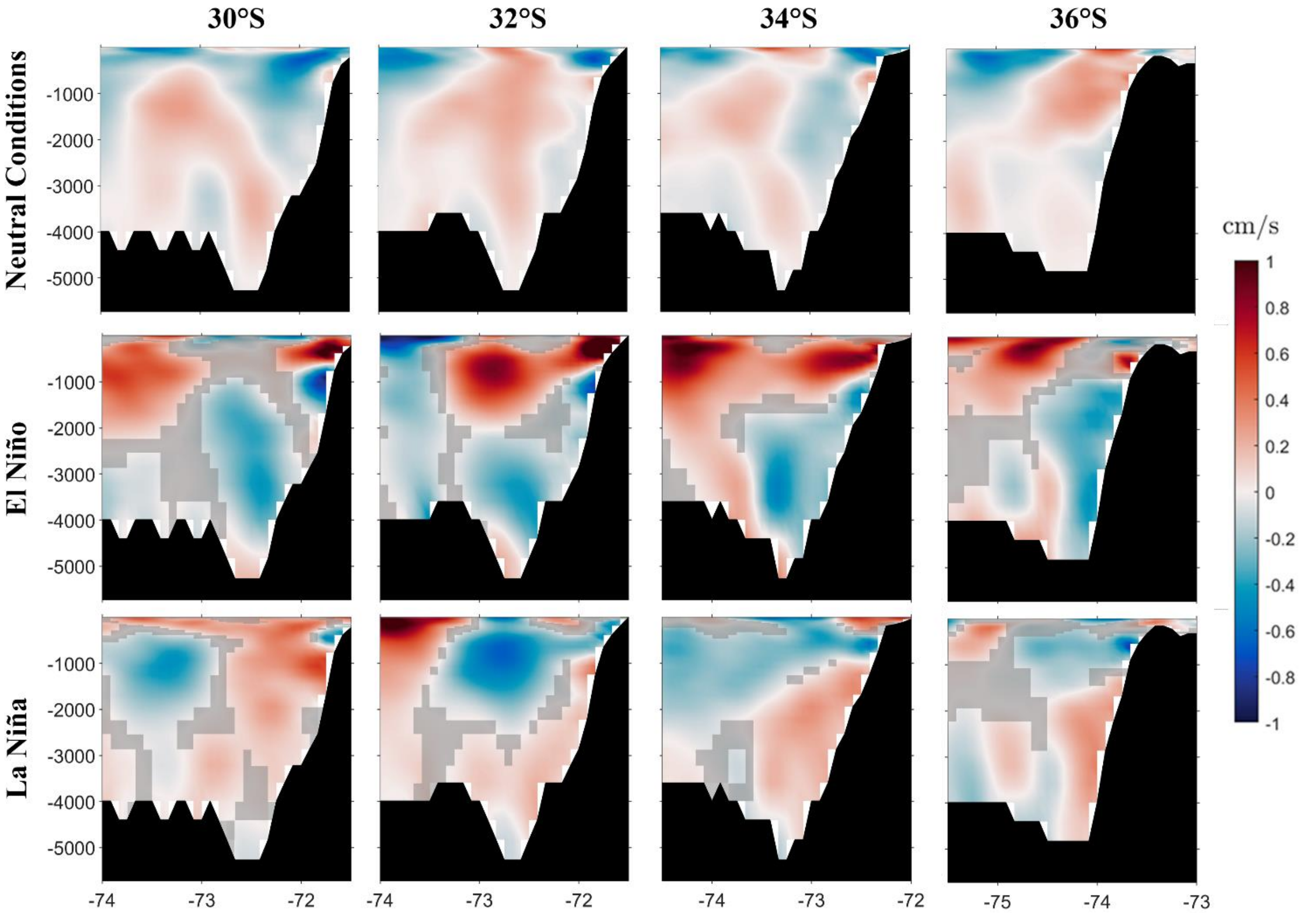

Figure 4. Anomalies of meridional velocity (cm/s) along the Chilean coast at four latitudes (30°S, 32°S, 34°S, and 36°S) under three different ENSO conditions, selected based on the MEI. The rows, from top to bottom, correspond to Neutral, El Niño, and La Niña periods. Positive values (red) indicate northward flow, while negative values (blue) indicate southward flow. Grey areas denote regions that are not statistically significant at the 95% confidence level, determined using a Montecarlo approach with 10.000 iterations.

https://doi.org/10.5194/egusphere-2025-1311
Preprint. Discussion started: 31 March 2025

Fig. 5 illustrates how the deep meridional current along the Chilean margin responds to large-scale interannual ENSO variability. At each of the four latitudes (30°S, 32°S, 34°S, and 36°S), the upper panels display correlation coefficients, and the lower panels display the corresponding regression coefficients. Red shading indicates currents that strengthen (i.e., have a positive relationship) when the MEI is high, whereas blue shading reflects an inverse relationship (i.e., negative correlation or regression). Only statistically significant regions (95% confidence) are shown, highlighting where ENSO-related signals penetrate the deep ocean. Note the inverse relationship with MEI below about 1500 m depth near the boundary, consistent with the time series of the meridional current plotted in Figs. 1 and 3.

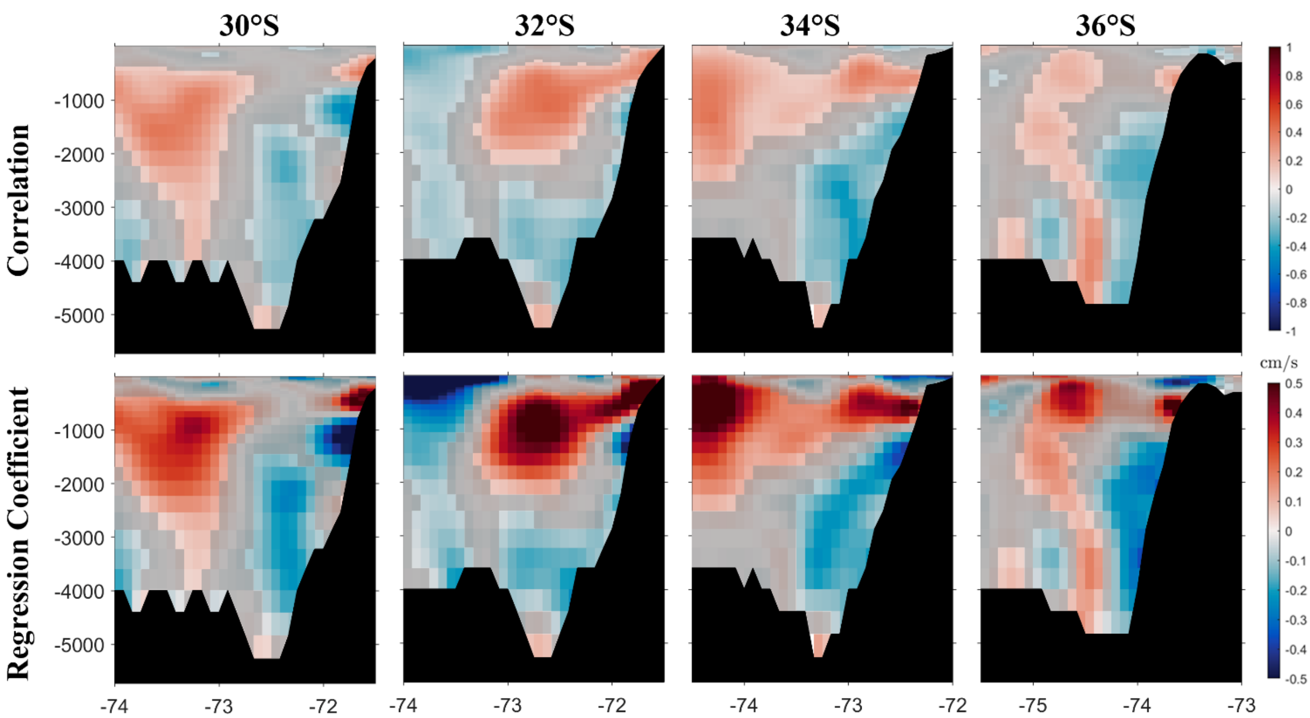

Figure 5. Correlation (*r*) and regression coefficients of the interannual meridional current against the Multivariate ENSO Index (MEI) at four latitudes along the Chilean coast (30°S, 32°S, 34°S, and 36°S). The top row shows correlation coefficients, while the bottom row shows regression coefficients. Grey areas indicate regions that are not statistically significant at the 95% confidence level using the p-value method.

To further analyze the long-term variability of this deep flow, we analyze longitude-time diagrams of interannual meridional velocity anomalies at depths close to 2000 m and 3000 m (Fig. 6). These velocity time series were compared with meridional subsurface velocity anomalies near the coast, averaged within the thermocline depth range (between about 220 and 450 m depth), as well as with interannual anomalies of the GLORYS sea level height (SLH). To highlight the relationship between low-frequency variability and ENSO cycles, El Niño and La Niña periods are indicated with red and blue rectangles,

https://doi.org/10.5194/egusphere-2025-1311
Preprint. Discussion started: 31 March 2025

respectively, based on the MEI time series (Fig. 6g). At both 2225 m and 3220 m depths, the diagrams reveal distinct bands of alternating positive (northward) and negative (southward) anomalies, indicating low-frequency variability. These anomalies suggest westward propagation, likely associated with the radiation of Rossby waves from the eastern boundary into the open ocean. On the other hand, SLH anomalies show coherent offshore propagation at a much faster speed. Positive (negative) SLH anomalies near the coast correspond to El Niño (La Niña) periods, underscoring the influence of ENSO on this variability. While SLH anomalies occur almost simultaneously between the coast and 76°W, likely due to rapid westward propagation (Fig. 6c), deep current anomalies at 2225 m and 3220 m depths show much slower westward propagating anomalies (Fig. 6a, b). The SLH anomalies are predominantly influenced by the first vertical mode, which propagates faster and more coherently westward. In contrast, subsurface and deep currents appear to be strongly affected by higher order baroclinic modes (cf. Figure 5 in Pizarro et al., 2001). The superposition of modes likely generates the more complex patterns observed in the longitude-time diagrams of current anomalies, contrasting with the simpler SLH variability. As higher modes propagate more slowly than lower modes, deep ocean current anomalies exhibit slower offshore propagation, as suggested by the diagrams of the deep flow in Fig. 6. The straight slanted line in Fig. 6b indicates a propagation speed of ~3×10^{-3} ms^{-1}. Note that the typical phase speed of the first, second and third modes of long Rossby wave in this region are about 1.6×10^{-2}, 4.8×10^{-3} and 2.3×10^{-3} m s^{-1}, respectively. This suggests that higher modes play a more significant role in the variability of deep currents compared to SLH variability.

https://doi.org/10.5194/egusphere-2025-1311
Preprint. Discussion started: 31 March 2025

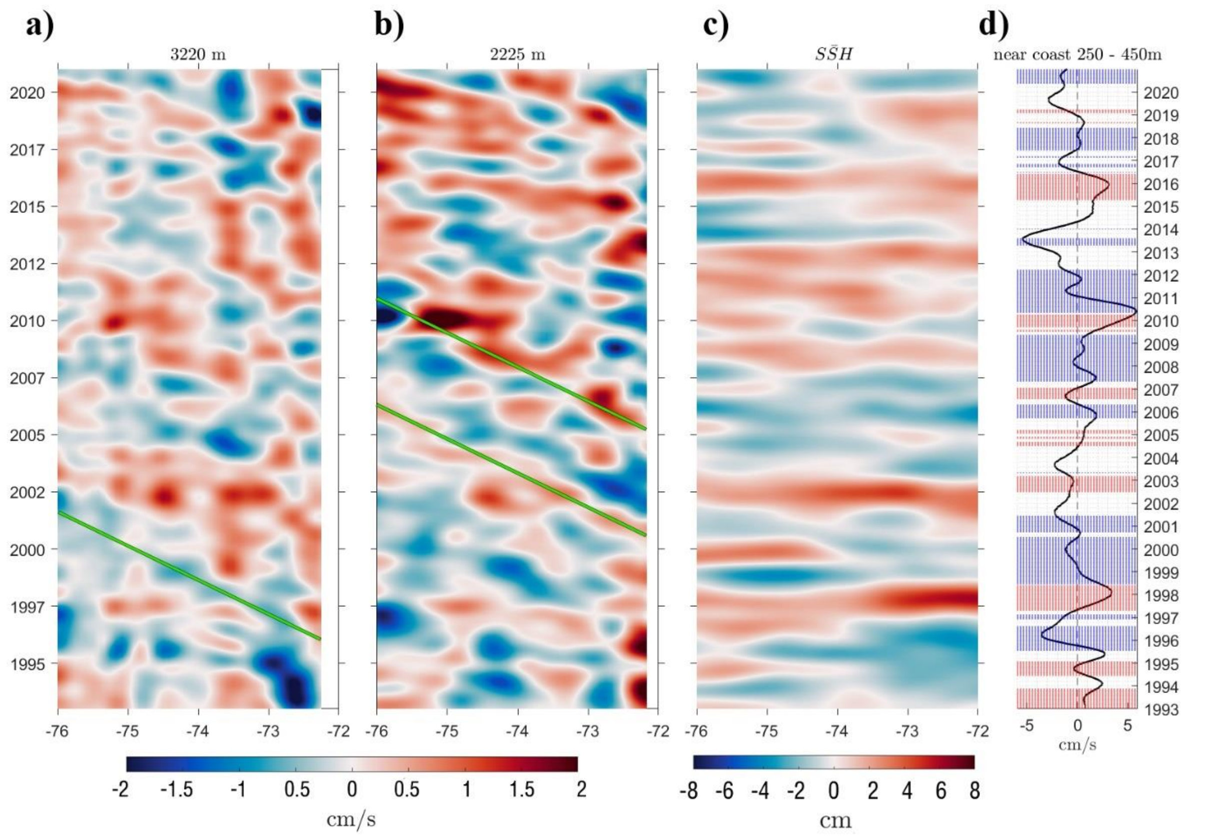

Figure 6: Longitude-time diagrams of interannual meridional velocity anomalies at 3000 m (a) and 2000 m (b). Velocities were averaged in the N-S direction between 31.5°S and 32.5°S. The Figure also shows the interannual anomalies of the sea surface height (c) and the meridional coastal velocities (d) averaged between 250 m and 450 m depth and from the continental slope to 25 km offshore. Red (blue) shaded in (d) indicates El Niño (La Niña) periods based on the MEI index. Green lines in a) and b) are used as a visual indicator of signal propagation.

Fig. 7 shows the low frequency time series of the meridional current anomalies in 3 different longitudes (72.5°, 73.5° and 74.5°W) at 32.5°S. Although the locations are relatively close (~94 km) the time series differ considerably between them, which is consistent with the variability observed in the longitude-time diagrams shown in Fig. 6. In the different selected sections shown in Fig. 7 there are periods where the phase shows an upward propagation; see for instance the period between 1995 and 2000 at 74.5°W (green line). To analyze this propagation, we use a simple vertical mode decomposition of the meridional current at 74.5°W using the model stratification and vertical dynamical modes. Details about the vertical mode decomposition and reconstruction are shown in the supplementary material. The reconstructed velocity pattern using the first 3 baroclinic modes plus a barotropic mode (Fig. B1) shows a vertical propagation pattern that is like the meridional velocity shown in Fig. 7d. The combination of baroclinic modes results in events of upward phase propagation. An upward phase

https://doi.org/10.5194/egusphere-2025-1311
Preprint. Discussion started: 31 March 2025

propagation is consistent with the downward propagation of the energy associated with baroclinic Rossby waves, which may transport energy from near surface or thermocline depths to the deep ocean.

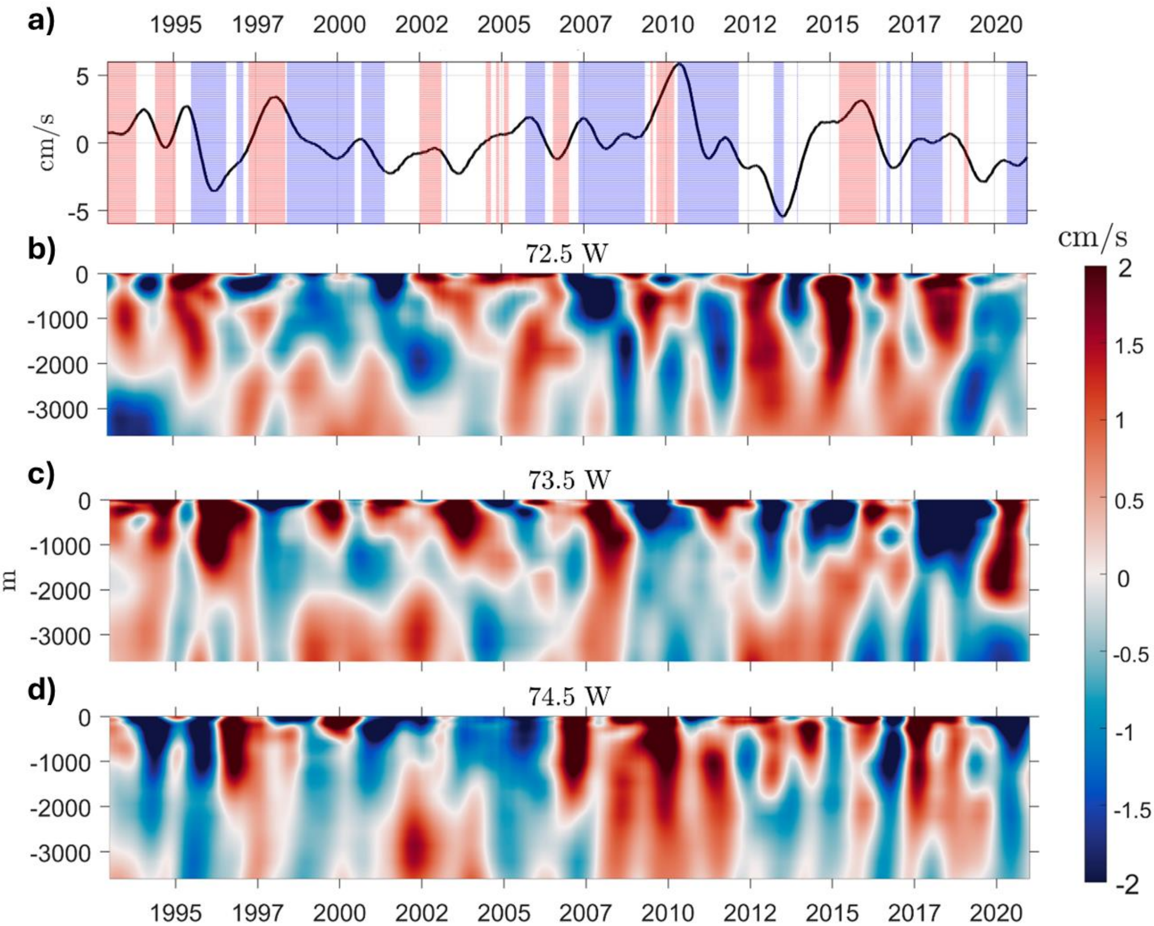

Figure 7. Interannual time series of the meridional velocity anomaly at 32°S and 72.5° (b), 73.5° (c) and 74.5°W (d) from GLORYS reanalysis. The panel (a) shows the interannual variability of the meridional velocity near the coast (averaged between 250 and 400 m depth, same as Fig. 6d) at 32°S.

To further examine the above findings, we apply complex empirical orthogonal functions (CEOF) to analyze the meridional current variability at 32.5°S near the eastern boundary. CEOF builds on the traditional EOF approach by incorporating both amplitude and phase information, making it especially useful for detecting propagating or wave-like signals. The first two CEOF modes explain approximately 31% and 27% of the interannual meridional current variance, respectively. Fig. 8a and b present the amplitude of these first two eigenvectors. Mode 1 shows stronger amplitudes below about 2500 m near the continental slope, as well as in the intermediate layer (above ~1500 m). In contrast, Mode 2 shows higher amplitudes

https://doi.org/10.5194/egusphere-2025-1311
Preprint. Discussion started: 31 March 2025

between roughly 1000 m and 3000 m above the trench, and near the bottom on the western side of the trench. Although the GLORYS12 reanalysis is not designed to analyze variability near the bottom in regions such as the Atacama Trench, the different structure in the variability observed here is consistent with geostrophic estimates (cf., Shulze & Speer, 2019).The principal component time series for Modes 1 and 2 are shown in Fig. 8c. Between 1993 and 2003, Mode 1 remains relatively steady, but then exhibits pronounced interannual variability characterized by distinct peaks and troughs—indicating periods of stronger or weaker activity. In contrast, Mode 2 displays considerable interannual variability throughout the entire study period. Neither of these modes shows a significant correlation with the MEI; however, both exhibit small yet significant coherence with climate indices associated with lower-frequency (decadal) variability, such as the Interdecadal Pacific Oscillation (IPO) and the Pacific Decadal Oscillation (PDO). A regression analysis with the IPO, analogous to the MEI analysis described above, is provided in Fig. C1. Larger correlations between IPO and the meridional current are observed above 2000 m over the trench.

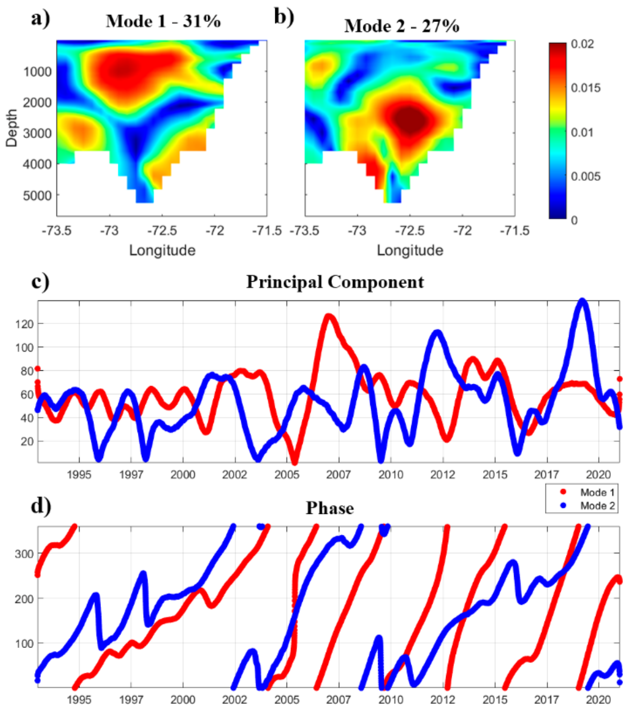

Figure 8. First and second Complex Empirical Orthogonal Function (CEOF) modes of the meridional velocity anomalies at 32°S normalized by its standard deviation. The eigen vector amplitude for modes 1 (a) and 2 (b), amplitude (c) and phase (d) time series for modes 1 (blue) and 2 (red) are shown. First and second modes explain 31% and 27% of the total variance of the normalized time series, respectively.

https://doi.org/10.5194/egusphere-2025-1311
Preprint. Discussion started: 31 March 2025

The phase time series for CEOF Modes 1 and 2 show that the original time series have dominant periodicities during most of the study period (Figure 8d), but there is a dominant oscillation captured by Mode 1 and Mode 2 of about 12 years (starting in 1993 and ending in 2004). After 2005 the dominant periods present in both modes are shorter between 2 and 5 years, consistent with the dominant period of ENSO. Together, both modes capture a substantial portion –about 58%– of the total variability of the interannual variability of the alongshore currents in the study region. The reconstruction of the alongshore current using mode 1 and 2 (Fig. 9) indicates an offshore-upward propagation from the deep slope over the continental margin and the trench.

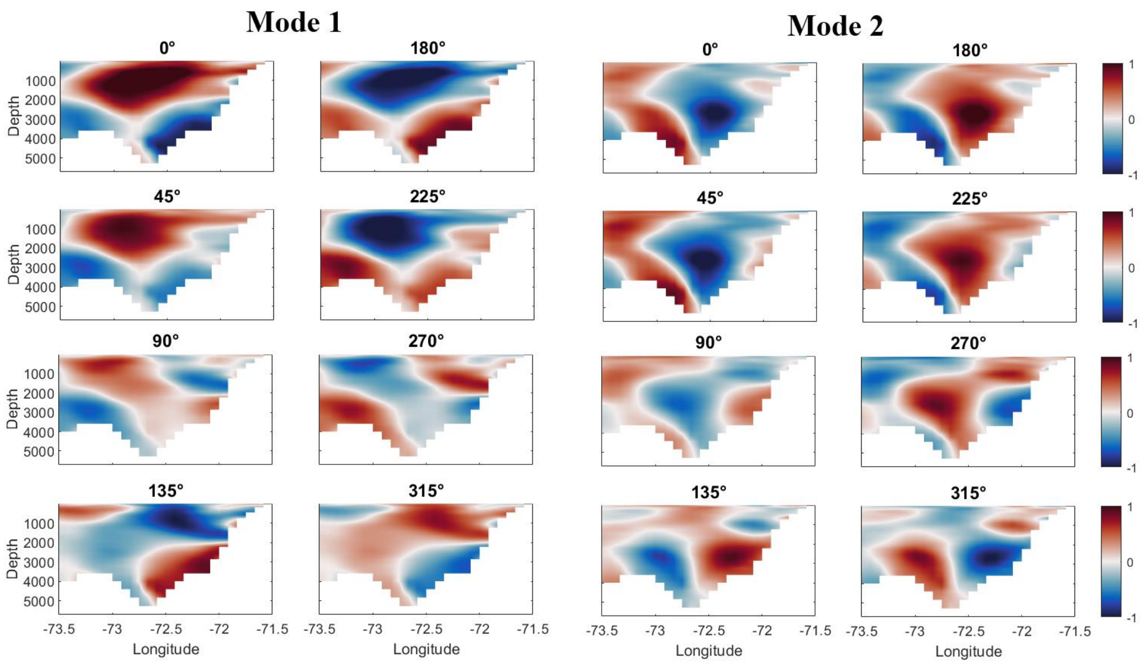

Figure 9. First and second CEOF modes of the meridional velocity anomalies at 32°S reconstructed for different phases shown in Fig 8d.

3.3 Eddy kinetic energy and Reynolds stresses

The deep southward flow remains spatially coherent along most of the continental margin off central Chile; however, notable spatial mesoscale variability appears in the CTZ between approximately 34°S and 37°S (Fig. 1a). This region coincides with an area of elevated eddy kinetic energy (EKE) in the deep current (Fig. 10, upper row), consistent with satellite-derived observations of strong surface mesoscale eddies (cf. Hormazabal et al., 2004). The pronounced maximum in deep EKE (2000–4000 m depth) is likely linked to mesoscale eddies that extend into the deep ocean (cf. Fig. 2).

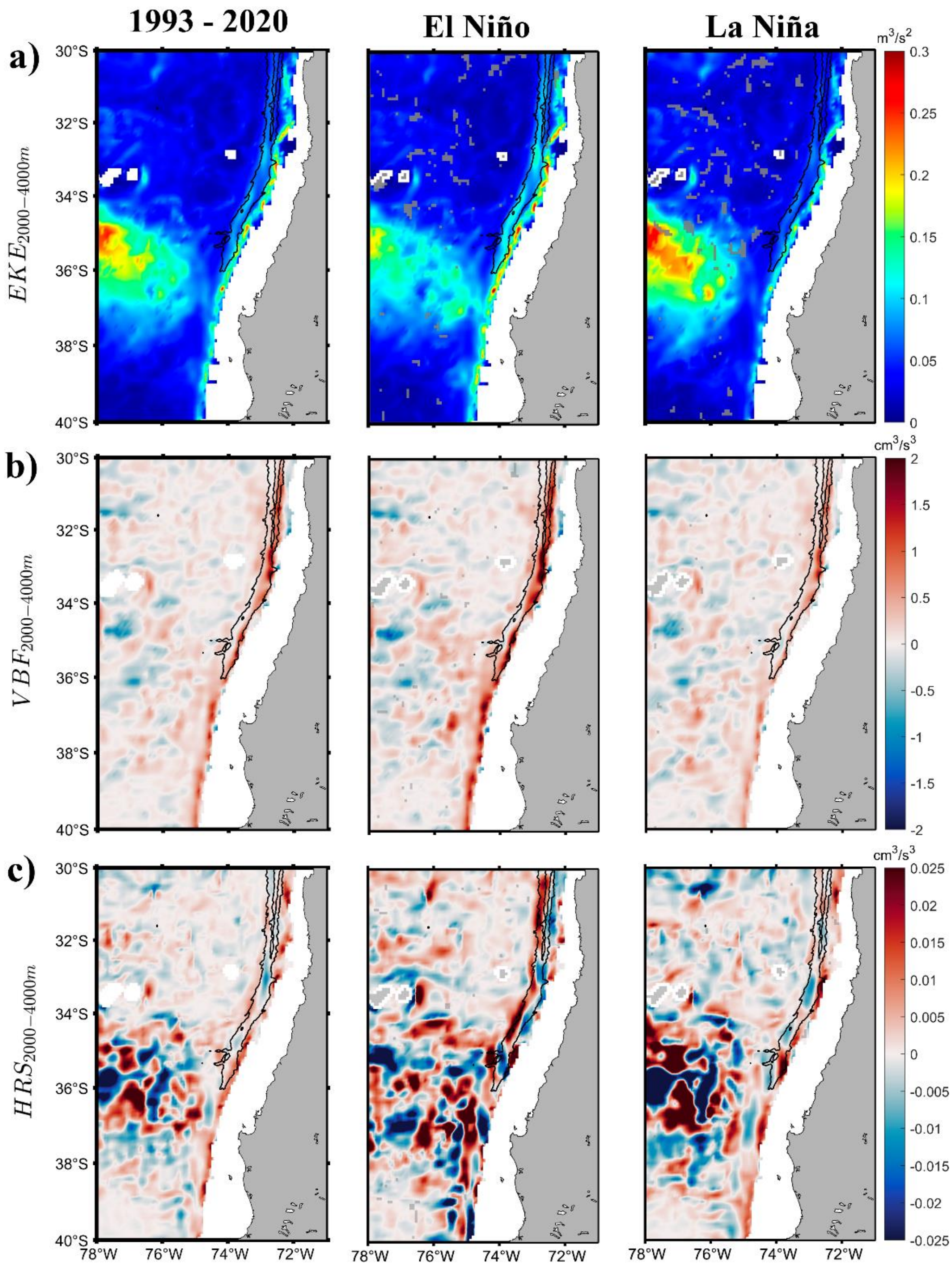

420 **Figure 10**: **Intraseasonal Eddy Kinetic Energy (EKE; a), Vertical Buoyancy Flux (VBF; b) and Horizontal Reynolds Stress (HRS; c) off Chile averaged between 2225 – 3992 m depth, for the whole period (left panels), El Niño (middle panels) and La Niña (right panels) periods. The black contours indicate the isobaths 5000 and 6000 m and locate the trench. Small grey areas mark regions of no statistical significance with a 95% confidence interval using a 10.000 iteration Montecarlo.**

https://doi.org/10.5194/egusphere-2025-1311
Preprint. Discussion started: 31 March 2025

Beyond the CTZ, relatively high EKE values also occur along the continental margin and on the western side of the trench, forming two nearly parallel bands (the coastal one being more intense than the other) that merge south of ~35°S, where the trench is largely filled with sediment and effectively disappears (e.g., Völker et al., 2006). When comparing different ENSO phases, deep EKE in the CTZ region tends to be higher during La Niña than during El Niño. In contrast, within the first ~100 km from the coast –covering the continental margin and the west side of the trench– EKE generally increases during El Niño (Table 1). This coastal increase is consistently observed across the multiple subregions depicted in Fig. 11 (coastal boxes).

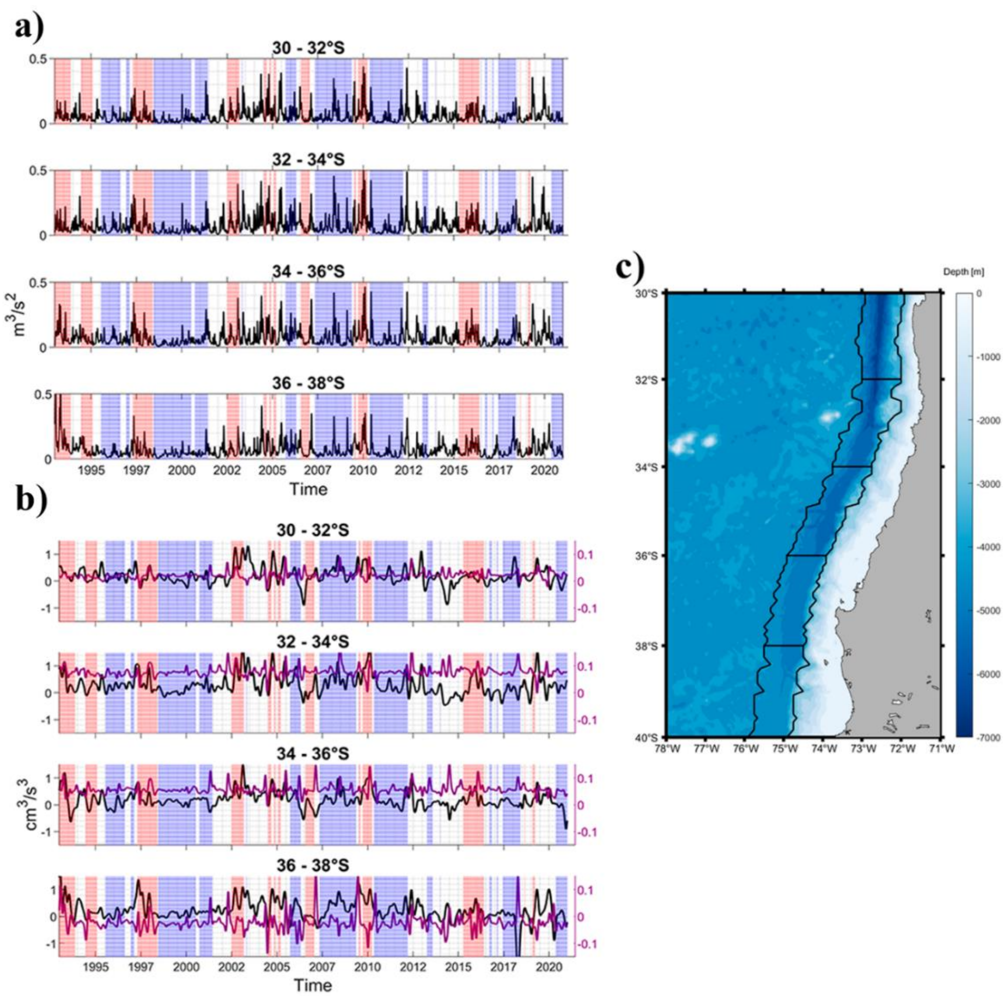

Figure 11: Intraseasonal a) Eddy Kinetic Energy, b) Vertical Buoyancy Flux (black) and Horizontal Reynolds Stress (purple) from the eastern South Pacific off Chile integrated between 2225 – 3992 m depth and averaged for each box represented in c). c) Bathymetry of the study region. The black contours represent the 5 boxes with a meridional length of 2° and a zonal thickness of 1°. The right side of each box is defined by the closest distance from the coast that has depths of over 2000 m. Blue (red) backgrounds in a) and b) indicate La Niña (El Niño) periods.

https://doi.org/10.5194/egusphere-2025-1311
Preprint. Discussion started: 31 March 2025

Along with EKE, we also calculate the horizontal and vertical Reynolds stresses (HRS and VRS, respectively) and the vertical buoyancy flux (VBF). Each of these quantities –HRS, VRS, and VBF– is integrated between 2225 and 3992 m depth. The third row of Fig. 10 shows the spatial distribution of HRS for the entire study period as well as for La Niña and El Niño phases. All three panels highlight higher magnitudes in areas similar to those of elevated EKE –namely, within the CTZ (approximately 34°S–37°S) and along both the continental margin and trench.

During the full record and La Niña periods, positive HRS dominates over the slope in the eastern side of the trench, whereas during El Niño conditions, large positive values appear mainly on the western side and negative values dominate the eastern side of the trench (Fig. 10). A positive HRS implies a transfer of energy from the mean flow to the intraseasonal variability, thereby enhancing the mean EKE ($\partial\overline{EKE}/\partial t > 0$). Conversely, negative HRS indicates that the intraseasonal variability transfers energy back into the mean flow, effectively strengthening the deep southward flow along the continental margin, while the opposite would be true on the seaward side of the trench. The VRS are one order of magnitude smaller than HRS and show similar spatial variability as HRS. In general, the VRS are mostly positive near the coast, with lower amplitudes in comparison to the oceanic region between about 35°S and 38°S (Fig. E1). The VBF shows predominant positive values in the CTZ and coastal region, with much larger values observed over the continental margin. There, VBF slightly increases during El Niño periods (Fig. 10; second row). In general, positive VBFs are consistent with EKE generation and with an increase of the southward flow as discussed below.

We selected four coastal boxes along the continental slope and the Atacama Trench (30°S–38°S) to evaluate the consistency of EKE, HRS, and VBF (Fig. 11). Although the standard deviations in each box are large –on the order of the mean itself– the mean EKE values remain remarkably similar along the latitudinal range (Table 1) with temporal means of vertically integrated (between 2225 – 3992 m) EKE ranging from 6.1×10^{-2} m³ s⁻² to 7.6×10^{-2} m³ s. In addition, higher EKE values coincide with El Niño periods (red shading in Fig. 11), whereas lower values are observed during La Niña (blue shading), a pattern that is confirmed by the ENSO phase-stratified estimates in Table 1. Meanwhile, HRS and VBF exhibit analogous along-slope coherence and comparable responsiveness to El Niño and La Niña conditions, underscoring the robust nature of these circulation patterns in the study region.

Both the HRS and the VBF exhibit clear responses to El Niño and La Niña events (Fig. 11, Table 1). Vertically integrated (2000–4000 m) HRS values lie in the range of 10^{-3} cm^3, while VBF reaches roughly two orders of magnitude higher (10^{-1} cm^3 s^{-3}, indicating that VBF is generally the larger contributor to the local EKE budget. Under El Niño conditions, both HRS and VBF tend to increase relative to La Niña periods, aligning with the enhanced deep circulation and buoyancy exchange observed during warm phases of ENSO. Across the four coastal boxes (30°S–38°S), their magnitudes remain relatively coherent in time –despite some latitudinal differences– underlining a consistent large-scale forcing effect. Notably,

https://doi.org/10.5194/egusphere-2025-1311
Preprint. Discussion started: 31 March 2025

standard deviations can be comparable to the mean, yet the overall rise (drop) in HRS and VBF during El Niño (La Niña) is evident in both the time series (Fig. 11) and the ENSO-stratified values presented in Table 1.

Table 1. Eddy Kinetic Energy (EKE), Horizontal Reynolds Stresses (HRS) and Vertical Buoyancy Fluxes (VBF) for different coastal boxes (see Figure 8) between 30°S and 40°S estimated for the whole period (2002-2018) and El Niño and la Niña periods. These periods were defined based on the Multivariate ENSO Index (MEI). All the values are vertically integrated between 2225 – 3992 m depth. The error is estimated as the standard deviation of the series.

Latitude °S	**EKE** (m^3 s^{-2}) ×10^{-2}			**HRS** (cm^3 s^{-3}) ×10^{-3}			**VBF** (cm^3 s^{-3}) ×10^{-1}		
	Total	**El Niño**	**La Niña**	**Total**	**El Niño**	**La Niña**	**Total**	**El Niño**	**La Niña**
30 - 32	6.1± 6.0	7.1± 6.3	4.8± 4.8	2.2± 19	2.9± 20	2.2± 14	2.0 ± 3.2	2.6 ± 3.1	1.6 ± 2.3
32 - 34	7.6 ± 6.9	8.7 ± 7.3	6.0± 5.8	2.0 ± 23	2.0 ± 25	1.9± 20	3.0 ± 3.7	4.7 ± 4.4	2.4 ± 2.5
34 - 36	7.4 ± 6.4	9.0 ± 7.3	5.9± 5.4	2.7 ± 19	3.2 ± 22	2.6± 15	1.9 ± 3.1	3.3 ± 4.0	0.9± 2.3
36 - 38	7.1± 6.2	9.4 ± 8.5	5.4± 4.7	3.3± 23	3.2 ± 25	2.5± 19	2.3 ± 3.9	3.9 ± 4.2	1.4 ± 3.6
Average 30 - 38	7.1±5.6	8.6±6.3	5.5±4.7	2.6±17	2.8±19	2.3±14	2.3±2.9	3.6±3.4	1.6±2.1

4 Discussion

4.1 The Deep Southward Flow off Chile

Since the pioneering evidence from Reid (1973) and Warren (1973), numerous observational and modeling studies have consistently identified a deep southward flow in the Chile Basin. Our results using the GLORYS Ocean Reanalysis further substantiate this flow, showing that it persists from about 2000 m to 4000 m depth along the eastern boundary of the South Pacific off Chile. The flow is predominantly southward, with a mean meridional transport of approximately -2.5 Sv near the continental margin, of which around 60% occurs within the first 100 km from the slope. This highlights the importance of continental margin dynamics in shaping the flow. Despite the presence of energetic mesoscale eddy activity, which can locally modulate the current, the long-term average flow remains robust and well-defined.

A synthesis of the different estimates of the southward transport in the Chile basin based on the different repetitions of the WOCE P06 Transect is presented in Table 2. There, different transport estimates are compared with our estimates based on GLORYS reanalysis. Despite significant variability among different estimates based on observations, there is consistent evidence of a deep southward flow transporting between 6 and 10 Sv in the whole Chile basin, from the East Pacific Rise to

https://doi.org/10.5194/egusphere-2025-1311
Preprint. Discussion started: 31 March 2025

the South American coast. Estimates based on the P06E line from 1992 (an El Niño year) indicated a stronger transport (~10 Sv) compared to those from 2003 and subsequent P06E repetitions (~6 Sv) (Schulze and Speer, 2019). While Arumí-Planas et al. (2022) use a level of no-motion (γn = 28.1 kg/m3) deeper than 3000 m, Schulze and Speer (2019) use a reference level based on the interface between the AAIW and PDW, typically located at around 1700 m depth in the region. Our transport estimates, based on GLORYS reanalysis, were notably smaller than those observed in P06E in 2003, 2010, and 2017. Nevertheless, a deep southward flow remained predominant along the eastern boundary in all cases. Note that the mean GLORYS transport for the period 1993-2020 was 4.0 Sv.

Overall, these findings build on previous work by demonstrating that the GLORYS reanalysis offers a reasonable representation of the deep southward transport and its variability, despite local discrepancies that can arise from eddy dynamics or different methodological choices (e.g., neutral density vs. potential density). Moreover, the interannual variability revealed in Section 3.1—where stronger southward transport coincides with El Niño phases—is consistent with earlier observational evidence (Shaffer et al., 1997, 2004; Schulze & Speer, 2019; Arumí-Planas et al., 2022). This variability underscores the influence of large-scale, low-frequency adjustments in the circulation, driven by remote equatorial forcing, on the deep flow along the Chilean margin.

Recent work by Yang et al. (2020a, 2020b, 2021) has significantly refined our understanding of Deep Eastern Boundary Currents (DEBC) observed in multiple ocean basins at depths of 2–4 km. In contrast to classical boundary-current theories dominated by wind forcing or western boundary dynamics (e.g., Stommel 1948: Munk, 1950), their studies demonstrate that topography and stratification are essential for sustaining DEBCs. A key mechanism is the vorticity balance between planetary vorticity advection and vortex stretching arising from lateral eddy temperature transport, which maintains the required density gradients against steep slopes or trenches. Notably, in their framework neither wind forcing nor surface buoyancy gradients are critical for driving these deep currents; instead, a combination of stratification, bottom topography, and friction establishes a narrow boundary layer and a broader interior-like flow. Their idealized and realistic numerical experiments further show that bathymetric features, particularly deep trenches, can lock DEBCs close to the boundary, while gentler slopes yield more diffuse currents. Taking together, these insights emphasize the importance of high-resolution models and accurate bathymetry for capturing DEBCs with significant implications for deep heat, carbon, and tracer transport and for improving future global climate simulations.

https://doi.org/10.5194/egusphere-2025-1311
Preprint. Discussion started: 31 March 2025

Table 2: Summary of the data, methodology and results obtained in circulation studies mentioned in the article.

Study	Data	Method	No motion level	Southward transport
Wijffels et al (2001) **W2001**	- P06 Hydrographic transect: 1992 - Current meters - Drifters	Inverse linear model	P = 3000 dbar	10 Sv
Shaffer et al (2004) **S2004**	- P06 Hydrographic transect: 1992 - Current meters	Geostrophic velocity calculation	**σ4 =** 45.83	9.5 Sv
Schulze and Speer (2019) **SS2019**	- P06, P17, P18, P19 and P21 hydrographic transects for all available periods - Lowered ADCP	Inverse model	P = 1700 dbar	6 Sv
Arumí-Planas et al (2022) **AP2022**	P06 hydrographic transects: 1992, 2003, 2010 and 2017	Inverse Box model of the Pacific Ocean	γ =28.1 kg/m^3	1992: 6.9 ± 4.9 Sv 2003: 5.3 ± 5.5 Sv 2010: 9.3 ± 5.0 Sv 2017: 8.5 ± 6.8 Sv
Present work 1: Observations	P06 Hydrographic transect: 1992: 2003, 2010 and 2017.	Geostrophic velocity calculation	γ = 28.05	1992: 6.57 Sv 2003: 4.97 Sv 2010: 4.93 Sv 2017: 5.87 Sv ± 0.68
Present work 2: Glorys12	Daily Glorys12 data averaged for the duration of the P06 2003, 2010 and 2017 repeats and for the 1993 - 2020 period	Meridional velocity from reanalysis	does not apply	2003: 3.74 Sv 2010: 0.94 Sv 2017: 1.44 Sv 1993 - 2020: 4.0 Sv

https://doi.org/10.5194/egusphere-2025-1311
Preprint. Discussion started: 31 March 2025

4.2 Rossby Waves and the Interannual Variability of the Deep Flow

The interplay of equatorial forcing and planetary wave dynamics has long been recognized as a driver of interannual fluctuations in coastal circulation off Chile (Shaffer et al., 1997, 2004; Pizarro et al., 2001; Dewitte et al., 2008). Our results, detailed in Section 3.2, show that El Niño events reinforce the deep southward flow, while La Niña phases weaken or even reverse it locally. During El Niño, the deep flow exhibits enhanced southward anomalies near the continental margin at depths below 1500 m, suggesting that large-scale, low-frequency adjustments in the circulation –triggered by remote equatorial forcing– can strengthen the deep southward flow along the slope. Conversely, La Niña phases typically show opposite flow anomalies, indicating a reduction of the deep southward component. Neutral conditions, on the other hand, exhibit much weaker anomalies, reflecting softened remote forcing.

Building on the composite and correlation analyses (Figs. 1, 3, 4, 5), our results underscore that deep, low-frequency anomalies often propagate westward and downward as Rossby waves, in line with earlier studies (Vega et al., 2003; Ramos et al., 2007; Vergara et al., 2017). The longitude-time diagrams of low-frequency meridional velocity anomalies at 2000 m and 3000 m depths reveal distinct bands of alternating positive (northward) and negative (southward) anomalies, suggesting westward propagation. While sea-level height (SLH) anomalies propagate offshore relatively rapidly –dominated by the first vertical baroclinic mode– meridional deep velocity anomalies at depth reveal more complex patterns. These patterns are more strongly influenced by higher baroclinic modes, which possess slower westward phase speeds and can induce vertical energy propagation from the thermocline down to deeper layers. The phase speed of the deep anomalies ($\sim 3\times10^{-3}$ m s^{-1}) aligns with the third vertical mode of long Rossby waves, highlighting the importance of higher modes in deep ocean variability. The upward phase propagation observed at certain longitudes (Section 3.2, Fig. 7) is consistent with downward energy transport associated with baroclinic Rossby waves, wherein multiple modes superimpose to shape the local velocity structure.

Results from the complex empirical orthogonal function (CEOF) analysis (Section 3.2, Figs. 8, 9) reinforce this multi-mode view. The leading modes exhibit pronounced interannual to decadal variability that is only weakly correlated with ENSO but shows some coherence with lower-frequency indices such as the Interdecadal Pacific Oscillation (IPO) and Pacific Decadal Oscillation (PDO). This indicates that the deep flow off Chile responds to both interannual-frequency (ENSO-related) and longer-term (PDO or IPO-related) climatic perturbations. Mode 1 of the CEOF analysis shows stronger amplitudes below 2500 m near the continental slope, while Mode 2 exhibits higher amplitudes between 1000 m and 3000 m above the trench. The principal component time series for these modes reveal distinct interannual variability, with Mode 1 showing pronounced peaks and troughs after 2003 and Mode 2 displaying considerable variability throughout the study period. Both modes exhibit a small yet significant coherence with the IPO, particularly above 2000 m over the trench (Fig. C1). This suggests that decadal-scale variability also plays a role in modulating the deep flow.

https://doi.org/10.5194/egusphere-2025-1311
Preprint. Discussion started: 31 March 2025

The vertical-mode decomposition further confirms that higher baroclinic modes can significantly modulate deep currents, sometimes leading to wave-like signals that differ markedly from the simpler SLH pattern at the surface. The reconstructed velocity pattern using the first three baroclinic modes plus a barotropic mode (Fig. B1) shows a vertical propagation pattern that is consistent with the meridional velocity anomalies observed in Figure 4. This upward phase propagation is consistent with the downward propagation of energy associated with baroclinic Rossby waves, which may transport energy from near-surface or thermocline depths to the deep ocean.

Taken together, these findings highlight that Rossby wave activity –particularly higher baroclinic modes– plays an integral role in coupling surface and thermocline signals with deep currents. This process can enhance southward deep flow during El Niño while reducing it during La Niña, thereby linking large-scale remote forcing to the local dynamics of the Chile Basin.

Since ENSO-induced Rossby wave forcing can modulate DEBC, it questions the extent to which it can also modulate the instability process that produces the energetic EKE activity there. While this has been shown for the PCUC (e.g., Conejero et al., 2021), our results suggest that this is also the case for the deep flow over the trench.

4.3 EKE Budget and Reynolds Stress Variability

Interactions between eddies and the mean flow may critically shape large-scale circulation in regions like the Chile Basin, where mesoscale variability is pronounced. We analyze these interactions via an eddy kinetic energy (EKE) budget, emphasizing how energy transfers occur between the mean flow and turbulent fluctuations. In particular, the horizontal and vertical Reynolds stresses (HRS and VRS) measure the conversion of mean Kinetic Energy to Eddy Kinetic energy through barotropic instabilities, while the vertical buoyancy flux (VBF) represents buoyancy-driven vertical exchanges that can alter stratification and induce vortex stretching. Together, these terms help explain how energy cascades across scales and how the mean deep flow adapts to mesoscale processes.

Our results reveal substantial EKE in the deep ocean (2000–4000 m), characterized by high spatial and temporal variability (Fig. 10, upper row). Larger values are observed near the continental slope and in the coastal transition zone (CTZ) between ~34°S and 37°S, coinciding with strong mesoscale eddies near the surface (Hormazabal et al., 2004). A pronounced maximum in deep EKE likely reflects mesoscale structures extending to depth, as suggested by the spatial coherence between EKE and eddy activity (cf. Figure 2). Beyond the CTZ, relatively high EKE also appears along the slope and on the western flank of the Atacama Trench, forming two nearly parallel bands that merge south of ~35-36°S, where the trench becomes buried by sediment (Völker et al., 2006).

https://doi.org/10.5194/egusphere-2025-1311
Preprint. Discussion started: 31 March 2025

ENSO phases prominently modulate EKE. During El Niño, EKE increases within ~100 km of the coast, encompassing the slope and the trench's western edge, whereas EKE in the CTZ tends to be higher during La Niña (Table 1). These patterns align with observed deep southward flow changes (Section 3.2): the flow intensifies in El Niño and weakens in La Niña. Consequently, enhanced EKE in El Niño conditions implies that mesoscale eddies more actively exchange energy with the mean flow under warm-phase period.

Analyses of HRS and VRS further illustrate complex mesoscale structures and energy exchanges. Positive HRS denotes energy transfer from the mean flow to intraseasonal variability, increasing EKE (∂(EKE)/∂t > 0), whereas negative HRS signifies the opposite: intraseasonal fluctuations reinforce the mean flow. During the full record and La Niña periods, positive HRS dominates the deep continental slope, but under El Niño, large positive HRS appears mainly on the western side of the trench, with negative values on the continental slope (Fig. 10c). These shifts underscore ENSO's control over which regions favor eddy growth versus mean flow strengthening. Although VRS amplitudes are roughly an order of magnitude smaller than HRS, they exhibit comparable spatial patterns, suggesting that vertical momentum exchanges also contribute to these dynamics. In contrast, VBF is often two orders of magnitude larger than HRS, showing predominantly positive values in the CTZ and coastal band –particularly over the continental margin. Positive VBF aligns with an increasing rate of change in EKE and with stronger southward flow. During El Niño, both HRS and VBF generally rise compared to La Niña, consistent with more vigorous deep circulation and buoyancy exchange (Fig. 7, bottom row).

Over the slope and trench, large positive VBF at intraseasonal timescales dominates between 2000 and 4000 m, overshading HRS and VRS. Here, the baroclinic deep southward flow is more intense, as indicated by the pronounced lowering of deep (~3000 m depth) isopycnals near the coast (Fig. 2). This downward displacement of density surfaces can be interpreted as vortex-tube stretching, reinforced by positive VBF that transports buoyancy upward and expands the isopycnal distance. As fluid layers gain buoyancy, they become less dense, forcing the isopycnals to spread apart. In a time-averaged sense, that expansion manifests as deeper isopycnals and stretching the vortex tubes, and ultimately a stronger southward flow.

Examination of EKE, HRS, and VBF across four coastal boxes (30°S–38°S) confirms their coherent variability (Figure 8, Table 1), with vertically integrated (between 2225 – 3992) EKE means ranging from 6.1×10^{-2} m^3 s^{-2} to 7.6×10^{-2} m^3 s^{-2}. Although the standard deviations of the EKE are large –on the order of the mean– EKE remains broadly similar across latitude, peaking during El Niño and dipping in La Niña. HRS and VBF mirror these ENSO-driven fluctuations, underscoring a robust regional response of deep eddy activity and buoyancy dynamics to large-scale climatic forcing.

Finally, the magnitude of intraseasonal VBF increases significantly over the Atacama Trench, surpassing both HRS and VRS. This suggests strong vertical motions and vortex stretching, which may potentially be balanced by the southward advection of planetary vorticity. Such processes support the strong EKE variability and the dynamics of the deep southward

https://doi.org/10.5194/egusphere-2025-1311
Preprint. Discussion started: 31 March 2025

flow, in line with previous findings that buoyancy-driven stretching is pivotal to deep boundary current systems (Yang et al., 2020, 2021). Altogether, these results demonstrate that ENSO forcing can substantially impact deep eddy–mean flow interactions in the Chile Basin, highlighting the need for high-resolution observations and models that accurately account for topography, baroclinic instabilities, and remote wave forcing to unravel the full complexity of deep EKE and its interplay with the mean flow. Although the ocean model used as part of the GLORYS reanalysis is not designed to analyze variability near the bottom or in regions with complex topography such as the Atacama Trench and the steep continental slope, our results are consistent with other studies, including studies based on direct observations and geostrophic estimates.

4.4 GLORYS12 Limitations

In addition to confirming the existence of the DESPC, this study provides an indirect evaluation of the natural variability present in this deep current. We identify 2 sources of variability: ENSO and instability processes, which are probably linked according to our results. There are some limitations in the GLORYS12 reanalysis. One is associated with time and the length of the simulation, where 28 years are insufficient to explain long term variability and having only 1 strong ENSO event that largely impacted the eastern Pacific (the 97-98 El Niño). The other limitation is the absence of a spatial grid adapted to the study of deep ocean. While GLORYS12 is an eddy resolving global model that is widely used for surface and subsurface oceanographic research, vertical resolution below 1000 m is coarse and deep and bottom circulation is highly dependent on bottom topography. Recent studies have shown that high-resolution usually tends to energize the mean deep circulation (e.g. Guo et al., 2024). Finally, due to scarce measurements at deep layers the model's circulation and dynamic is not constrained at these depths. Future work will consist in using a high-resolution regional model to better estimate the magnitude of intrinsic variability considering details in the bathymetry.

5 Summary and conclusion

In this study, we investigated the ENSO-driven variability of the deep southward flow in the Southeastern Pacific using the GLORYS12 ocean reanalysis (1993–2020), along with hydrographic data from repeated GO-SHIP/WOCE P06 transects. Our analysis focused on depths of approximately 2000–4000 m in the Chile Basin and adjacent areas, encompassing steep continental slopes and the Atacama Trench. The main findings can be summarized as follows:

We confirmed the existence of a robust southward flow at depths below ~2000 m near the Chilean continental margin. This flow –referred to as the Deep Eastern South Pacific Current (DESPC)– transports, on average, about 2.5 Sv within ~300 km of the coast. Approximately 60% of that transport is concentrated in the first 100 km next to the margin. Comparisons with GO-SHIP sections reveal that, despite eddy-induced fluctuations, the long-term behavior of the reanalysis-based current fields is broadly consistent with in situ estimates. These results add to existing observational and modeling evidence (Shaffer

https://doi.org/10.5194/egusphere-2025-1311
Preprint. Discussion started: 31 March 2025

et al., 2004; Schulze & Speer, 2019; Arumí-Planas et al., 2022) that the DESPC is a persistent feature in the Southeast Pacific and likely an integral part of the Pacific Meridional Overturning Circulation outflow.

The deep southward flow exhibits considerable interannual variability. Composites of El Niño and La Niña events show a systematic response: the flow strengthens (more negative meridional velocity) during El Niño and weakens during La Niña. Statistical analyses and correlation with the Multivariate ENSO Index indicate that these variations are driven, in part, by remote equatorial forcing transmitted along the coast and into the deep ocean. Our results highlight that ENSO-related fluctuations can extend below 2000 m, underscoring the role of low-frequency extratropical Rossby waves in communicating surface and near-thermocline anomalies down into the deep ocean. Longitude-time diagrams and a complex empirical orthogonal function (CEOF) analysis reveal slow westward propagation of velocity anomalies at 2000–3000 m depth, consistent with the phase speeds of higher baroclinic modes of long Rossby waves. Unlike sea level height (SLH) signals, which propagate more rapidly (dominated by the first baroclinic mode), the deeper currents display multi-modal variability and sometimes exhibit upward phase propagation. This behavior emphasizes the importance of higher-mode baroclinic processes in shaping deep-ocean responses to large-scale climate forcing in eastern boundary regions. Our results support the view that deep currents along eastern boundaries are crucial for global overturning and for connecting low-latitude and polar processes. ENSO exerts a pronounced influence, but we also detect longer-term (decadal) variability in the meridional. Such lower-frequency signals likely reflect the superposition of multiple modes, demonstrating that an accurate understanding of deep circulation requires capturing both interannual and decadal time scales.

The eddy kinetic energy (EKE) is enhanced along the continental slope, over the trench, and in specific offshore regions (the coastal transition zone between ~34°S and 37°S). By examining Reynolds stresses and vertical buoyancy fluxes (VBF), we identified energetic exchanges between mean and eddy fields. In particular, vertical buoyancy fluxes emerge as a key driver of elevated EKE in the deep ocean, transferring available potential energy to eddy kinetic energy and thus modulating mean flows. While both horizontal and vertical Reynolds stresses (HRS and VRS) contribute to these energy exchanges, the VBF can be notably larger, especially near the slope and during El Niño events.

Direct measurements of velocity, stratification, and mixing in the 2000–4000 m range remain sparse. Additional extended current-meter and CTD deployments, and dedicated repeat hydrographic surveys would improve our understanding of the mechanisms driving interannual to decadal variability of the DESPC. The interaction of steep slopes, trenches, and eddy-resolving mesoscale dynamics poses significant challenges for global ocean models and reanalyses. Efforts to reduce model biases, incorporate improved bathymetric data, and refine parameterizations of eddy–mean flow interactions are needed to capture the full complexity of deep circulation.

https://doi.org/10.5194/egusphere-2025-1311
Preprint. Discussion started: 31 March 2025

Overall, our findings underscore the importance of the deep southward flow off Chile as an integral pathway in the meridional overturning circulation of the Pacific. The interplay of local topography, mesoscale processes, and remote climatic forcing via ENSO and Rossby waves proves essential for modulating its variability. In the broader context of Pacific circulation, these insights emphasize the need for high-resolution modeling and sustained in situ observations, like the deep ARGO project (Zilberman et al., 2023) and the Integrated Deep-Ocean Observing System (IDOOS) located over the Atacama Trench (Ulloa et al., 2023), to fully characterize the dynamics of the deep eastern boundary current system and its sensitivity to climate variability.

https://doi.org/10.5194/egusphere-2025-1311
Preprint. Discussion started: 31 March 2025

700 **Appendix A. Frequency Spectrum**

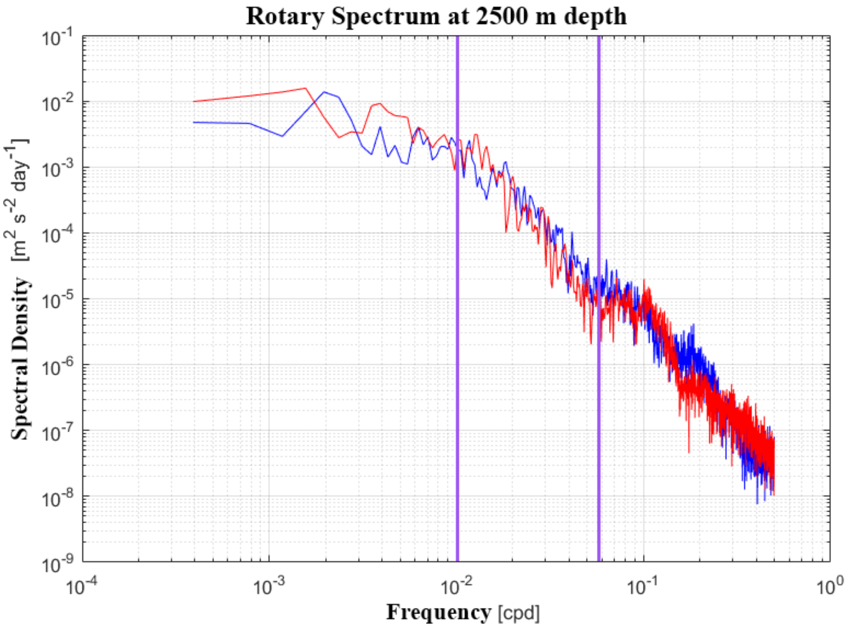

Figure A1 Rotary spectrum of meridional velocity from 2500 m at 30.08°S, 73.3° W

Appendix B. Baroclinic Mode Reconstruction

705 To obtain the structure of the baroclinic modes we used the dynmodes function in MATLAB developed by J. Klinck (1999). These modes describe the natural oscillations that appear in a stratified fluid due to the interaction between gravity effects and density gradients, being crucial to understanding the vertical structure of the ocean circulation and its response to different forcing.

The frequency of each mode of a Rossby wave is associated with the propagation velocity of the vertical mode (c_n), which 710 in turn corresponds to the phase velocity of a long baroclinic gravity wave) through the dispersion relation. For example, for a long Rossby wave, this is simply

$$\omega_n = -\beta k (c_n/f)^2$$

The typical phase speed of the first, second and third modes of long Rossby wave in this region are 1.6×10^{-2}, 4.8×10^{-3} and 2.3×10^{-3} m s^{-1}, respectively.

https://doi.org/10.5194/egusphere-2025-1311
Preprint. Discussion started: 31 March 2025

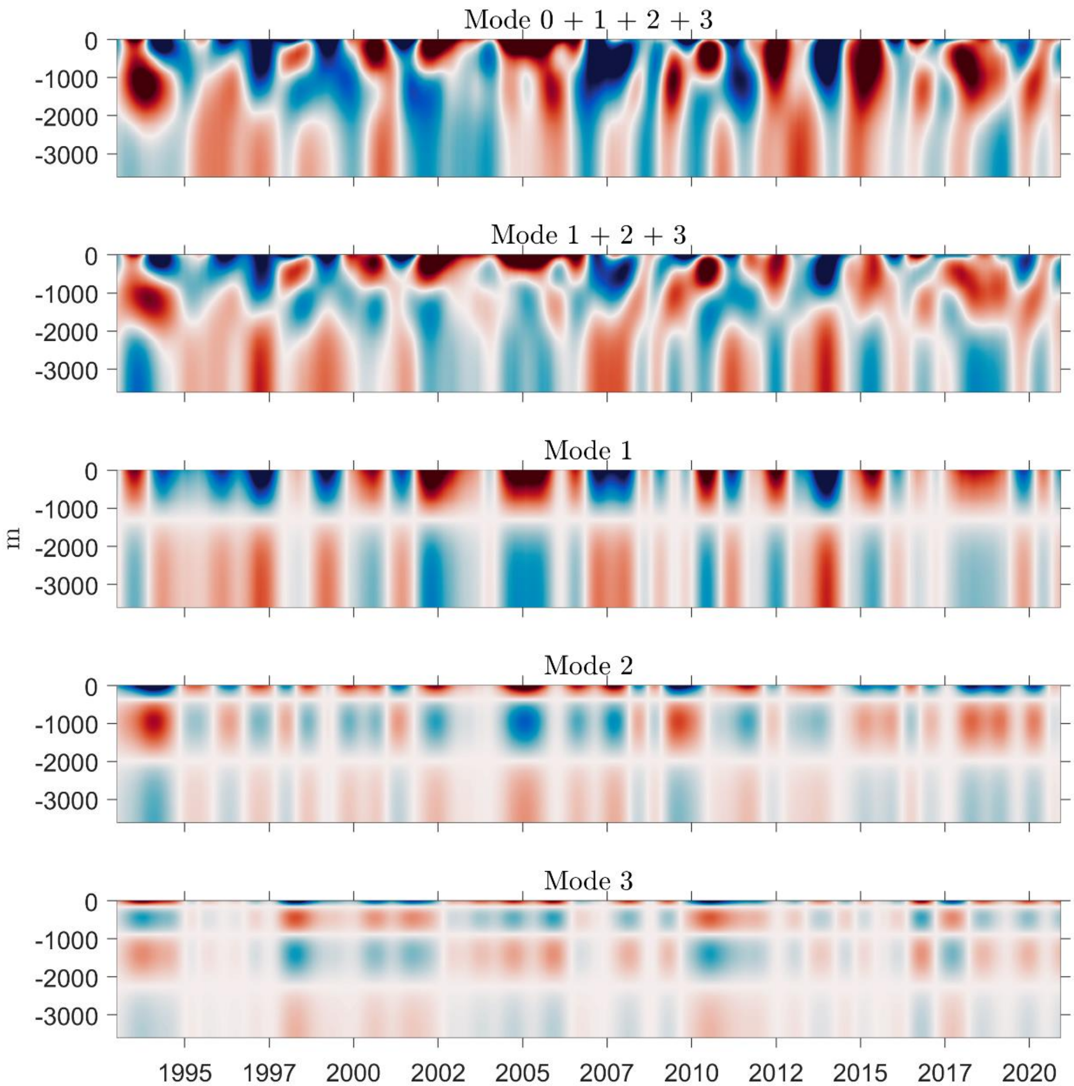

715

Figure B1 Interannual time series of the meridional velocity anomaly at 74.5°W, 32°S reconstructed using a barotropic mode (mode 0) and the first 3 baroclinic modes.

https://doi.org/10.5194/egusphere-2025-1311
Preprint. Discussion started: 31 March 2025

720 **Appendix C. Interdecadal Pacific Oscillation**

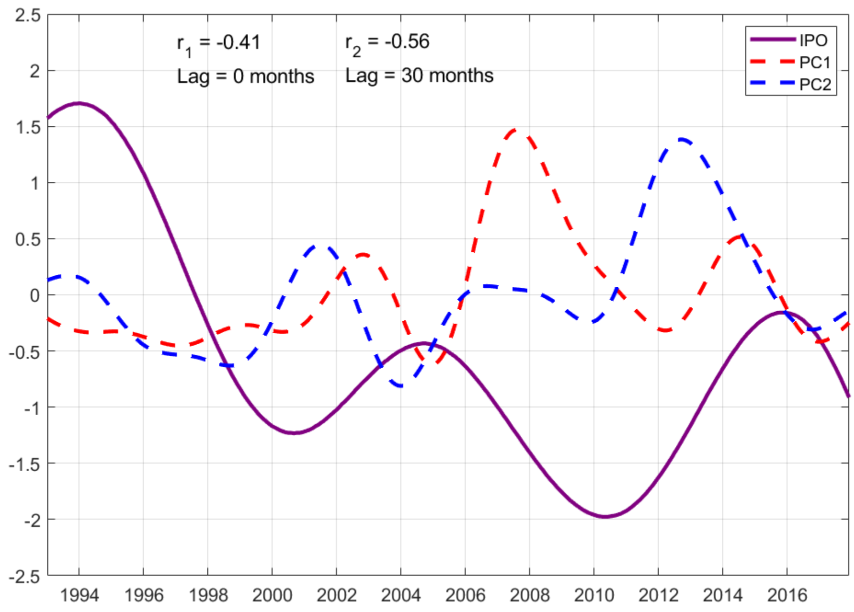

Figure C1. Interdecadal Pacific Oscillation (IPO) normalized principal components of mode 1 and 2 of the CEOF of deep meridional flow shown in Fig. 8c. r1 and r2 correspond to the correlation between IPO and PC1 and PC2 respectively, IPO leads PC2.. Both PCs were low pass filtered using a 5-year Hamming filter to remove some interannual frequencies.

725

https://doi.org/10.5194/egusphere-2025-1311
Preprint. Discussion started: 31 March 2025

Appendix D. Surface EKE

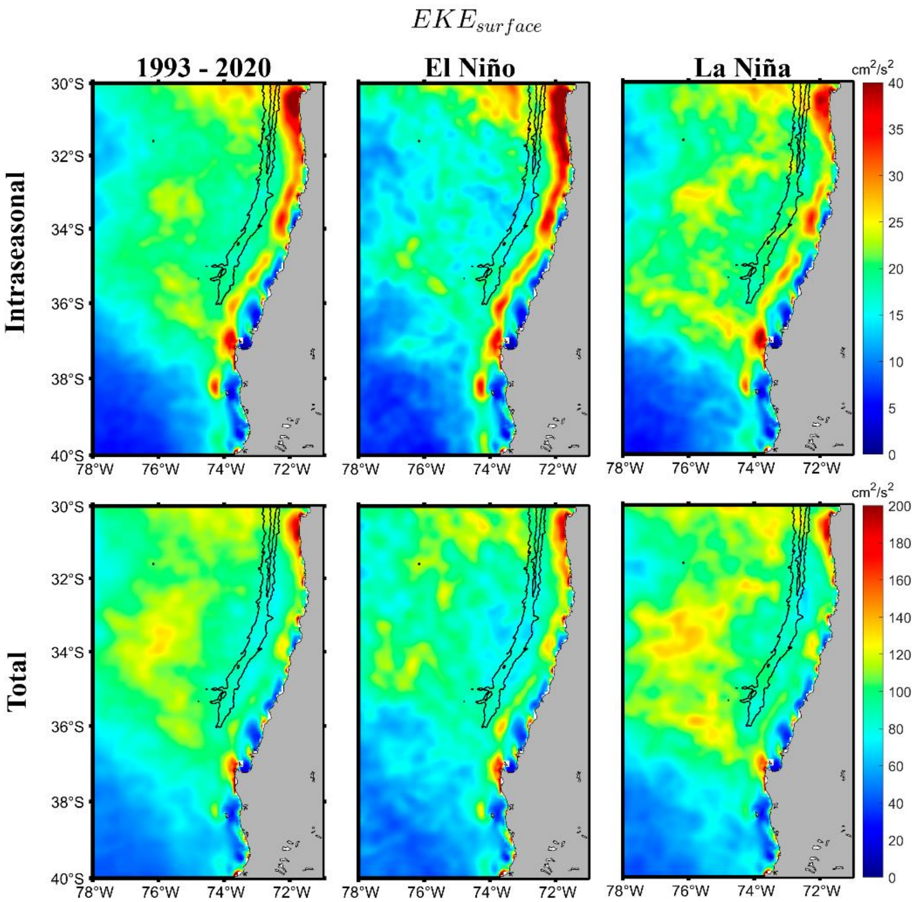

Figure D1. Intraseasonal (upper row) and total (lower row) Eddy Kinetic Energy in the first layer of the GLORYS12 reanalysis ~0.5 m depth, for the whole period (left panel), El Niño (middle panel) and La Niña (right panel) periods. Total EKE was calculated using the anomaly time series (SA) of zonal and meridional velocities.

https://doi.org/10.5194/egusphere-2025-1311
Preprint. Discussion started: 31 March 2025

Appendix E. Vertical Reynolds Stress

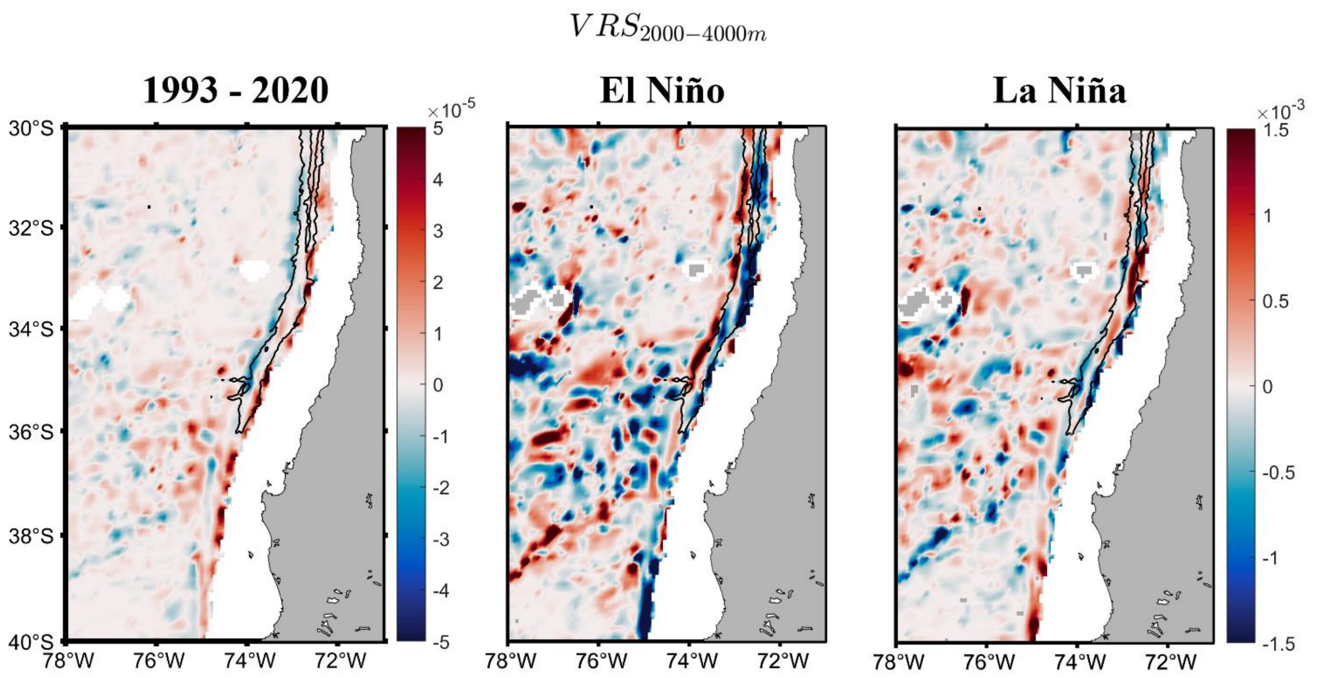

Figure E1. Intraseasonal Vertical Reynolds Stress off Chile averaged between 2225 – 3992 m depth, for the whole period (left panel), El Niño (middle panel) and La Niña (right panel) periods.

Author contributions

MTG: Analysis, data processing, methodology and writing. OP: Analysis, writing and methodology. BD and VO: analysis methodology and writing.

Competing interests

The contact author has declared that none of the authors has any competing interests.

Financial support

This research was supported by the Millennium Institute of Oceanography (IMO, ICN12_019) and CLAP project (Concurso de Fortalecimiento al Desarrollo Científico de Centros Regionales 2020-R20F0008-CEAZA).

Acknowledgement

MT was supported by Agencia Nacional de Investigación y Desarrollo (ANID) Chile by the Magister Nacional scholarship and by scholarship from IMO. BD also acknowledges support from Centro de Investigación Oceanográfica en el Pacífico Sur-Oriental COPAS COASTAL FB210021. OP thanks support from Poste Rouge and CECI during a sabbatical stance (August 2024-January 2025) in Toulouse France as part of a collaboration between University of Toulouse III, LEGOS, IRD, CECI and the University of Concepción. We use DeepL to help us with the wording.

References

Arumí-Planas, C., Hernández-Guerra, A., Caínzos, V., Vélez-Belchí, P., Farneti, R., Mazloff, M. R., Mecking, S., Rosso, I., Schulze Chretien, L. M., Speer, K. G., & Talley, L. D. (2022). Variability in the meridional overturning circulation at 32°S in the Pacific Ocean diagnosed by inverse box models. *Progress in Oceanography*, *203*, 102780. https://doi.org/10.1016/j.pocean.2022.102780

Broeker, W. (1991). The Great Ocean Conveyor. *Oceanography*, *4*(2), 79-89. https://doi.org/10.5670/oceanog.1991.07

Burls, N. J., Fedorov, A. V., Sigman, D. M., Jaccard, S. L., Tiedemann, R., & Haug, G. H. (2017). Active Pacific meridional overturning circulation (PMOC) during the warm Pliocene. *Science Advances*, *3*(9), e1700156. https://doi.org/10.1126/sciadv.1700156

Chaigneau, A., Pizarro, O., & Rojas, W. (2008). Global climatology of near-inertial current characteristics from Lagrangian observations. *Geophysical Research Letters*, *35*(13), 2008GL034060. https://doi.org/10.1029/2008GL034060

Conejero, C., Dewitte, B., Garçon, V., Sudre, J., & Montes, I. (2020). ENSO diversity driving low-frequency change in mesoscale activity off Peru and Chile. *Scientific Reports*, *10*(1), 17902. https://doi.org/10.1038/s41598-020-74762-x

Contreras, M., Pizarro, O., Dewitte, B., Sepulveda, H. H., & Renault, L. (2019). Subsurface Mesoscale Eddy Generation in the Ocean off Central Chile. *Journal of Geophysical Research: Oceans*, *124*(8), 5700-5722. https://doi.org/10.1029/2018JC014723

Curtis, P. E., & Fedorov, A. V. (2024). Spontaneous Activation of the Pacific Meridional Overturning Circulation (PMOC) in Long-Term Ocean Response to Greenhouse Forcing. *Journal of Climate*, *37*(5), 1551-1565. https://doi.org/10.1175/JCLI-D-23-0393.1

Dewitte, B., Conejero, C., Ramos, M., Bravo, L., Garçon, V., Parada, C., Sellanes, J., Mecho, A., Muñoz, P., & Gaymer, C. F. (2021). Understanding the impact of climate change on the oceanic circulation in the Chilean island ecoregions. *Aquatic Conservation: Marine and Freshwater Ecosystems*, *31*(2), 232-252. https://doi.org/10.1002/aqc.3506

https://doi.org/10.5194/egusphere-2025-1311
Preprint. Discussion started: 31 March 2025

Dewitte, B., Purca, S., Illig, S., Renault, L., & Giese, B. S. (2008). Low-Frequency Modulation of Intraseasonal Equatorial Kelvin Wave Activity in the Pacific from SODA: 1958–2001. *Journal of Climate*, *21*(22), 6060-6069. https://doi.org/10.1175/2008JCLI2277.1

Ferreira, D., Cessi, P., Coxall, H. K., De Boer, A., Dijkstra, H. A., Drijfhout, S. S., Eldevik, T., Harnik, N., McManus, J. F., Marshall, D. P., Nilsson, J., Roquet, F., Schneider, T., & Wills, R. C. (2018). Atlantic-Pacific Asymmetry in Deep Water Formation. *Annual Review of Earth and Planetary Sciences*, *46*(1), 327-352. https://doi.org/10.1146/annurev-earth-082517-010045

Guo, H., Chen, Z., Zhu, R., & Cai, J. (2024). Increasing model resolution improves but overestimates global mid-depth circulation simulation. *Scientific Reports*, *14*(1), 29356. https://doi.org/10.1038/s41598-024-80152-4

Harrison, D. E., & Robinson, A. R. (1978). Energy analysis of open regions of turbulent flows—Mean eddy energetics of a numerical ocean circulation experiment. *Dynamics of Atmospheres and Oceans*, *2*(2), 185-211. https://doi.org/10.1016/0377-0265(78)90009-X

Hernández-Guerra, A., & Talley, L. D. (2016). Meridional overturning transports at 30°S in the Indian and Pacific Oceans in 2002–2003 and 2009. *Progress in Oceanography*, *146*, 89-120. https://doi.org/10.1016/j.pocean.2016.06.005

Hogg, A. M. C., Dewar, W. K., Berloff, P., Kravtsov, S., & Hutchinson, D. K. (2009). The Effects of Mesoscale Ocean–Atmosphere Coupling on the Large-Scale Ocean Circulation. *Journal of Climate*, *22*(15), 4066-4082. https://doi.org/10.1175/2009JCLI2629.1

Holbourn, A., Kuhnt, W., Kulhanek, D. K., Mountain, G., Rosenthal, Y., Sagawa, T., Lübbers, J., & Andersen, N. (2024). Re-organization of Pacific overturning circulation across the Miocene Climate Optimum. *Nature Communications*, *15*(1), 8135. https://doi.org/10.1038/s41467-024-52516-x

Hormazabal, S., Shaffer, G., & Leth, O. (2004). Coastal transition zone off Chile. *Journal of Geophysical Research: Oceans*, *109*(C1), 2003JC001956. https://doi.org/10.1029/2003JC001956

Jackett, D. R., & McDougall, T. J. (1997). A Neutral Density Variable for the World's Oceans. *Journal of Physical Oceanography*, *27*(2), 237-263. https://doi.org/10.1175/1520-0485(1997)027<0237:ANDVFT>2.0.CO;2

Jean-Michel, L., Eric, G., Romain, B.-B., Gilles, G., Angélique, M., Marie, D., Clément, B., Mathieu, H., Olivier, L. G., Charly, R., Tony, C., Charles-Emmanuel, T., Florent, G., Giovanni, R., Mounir, B., Yann, D., & Pierre-Yves, L. T. (2021). The Copernicus Global 1/12° Oceanic and Sea Ice GLORYS12 Reanalysis. *Frontiers in Earth Science*, *9*, 698876. https://doi.org/10.3389/feart.2021.698876

Kawabe, M., & Fujio, S. (2010). Pacific Ocean circulation based on observation. *Journal of Oceanography*, *66*(3), 389-403. https://doi.org/10.1007/s10872-010-0034-8

Klinck, J. (1999). *Dynmodes* [Matlab]. https://github.com/sea-mat/dynmodes/blob/master/dynmodes.m

Klocker, A., & McDougall, T. J. (2010). Influence of the Nonlinear Equation of State on Global Estimates of Dianeutral Advection and Diffusion. *Journal of Physical Oceanography*, *40*(8), 1690-1709. https://doi.org/10.1175/2010JPO4303.1

https://doi.org/10.5194/egusphere-2025-1311
Preprint. Discussion started: 31 March 2025

Leth, O., Shaffer, G., & Ulloa, O. (2004). Hydrography of the eastern South Pacific Ocean: Results from the Sonne 102 cruise, May–June 1995. *Deep Sea Research Part II: Topical Studies in Oceanography*, *51*(20-21), 2349-2369. https://doi.org/10.1016/j.dsr2.2004.08.009

Li, Z., Groeskamp, S., Cerovečki, I., & England, M. H. (2022). The Origin and Fate of Antarctic Intermediate Water in the Southern Ocean. *Journal of Physical Oceanography*, *52*(11), 2873-2890. https://doi.org/10.1175/JPO-D-21-0221.1

Linford, P., Pérez-Santos, I., Montes, I., Dewitte, B., Buchan, S., Narváez, D., Saldías, G., Pinilla, E., Garreaud, R., Díaz, P., Schwerter, C., Montero, P., Rodríguez-Villegas, C., Cáceres-Soto, M., Mancilla-Gutiérrez, G., & Altamirano, R. (2023). Recent Deoxygenation of Patagonian Fjord Subsurface Waters Connected to the Peru–Chile Undercurrent and Equatorial Subsurface Water Variability. *Global Biogeochemical Cycles*, *37*(6), e2022GB007688. https://doi.org/10.1029/2022GB007688

Montecinos, A., & Pizarro, O. (2005). Interdecadal sea surface temperature–sea level pressure coupled variability in the South Pacific Ocean. *Journal of Geophysical Research: Oceans*, *110*(C8), 2004JC002743. https://doi.org/10.1029/2004JC002743

Munk, W. H. (1950). ON THE WIND-DRIVEN OCEAN CIRCULATION. *Journal of Atmospheric Sciences*, *7*(2), 80-93. https://doi.org/10.1175/1520-0469(1950)007<0080:OTWDOC>2.0.CO;2

Pizarro, O., Clarke, A. J., & Van Gorder, S. (2001). El Niño Sea Level and Currents along the South American Coast: Comparison of Observations with Theory. *Journal of Physical Oceanography*, *31*(7), 1891-1903. https://doi.org/10.1175/1520-0485(2001)031<1891:ENOSLA>2.0.CO;2

Ramos, M., Dewitte, B., Pizarro, O., & Garric, G. (2008). Vertical propagation of extratropical Rossby waves during the 1997–1998 El Niño off the west coast of South America in a medium-resolution OGCM simulation. *Journal of Geophysical Research: Oceans*, *113*(C8), 2007JC004681. https://doi.org/10.1029/2007JC004681

Reid, J. L. (1973). Transpacific hydrographic sections at Lats. 43°S and 28°S: The SCORPIO expedition—III. Upper water and a note on southward flow at mid-depth. *Deep Sea Research and Oceanographic Abstracts*, *20*(1), 39-49. https://doi.org/10.1016/0011-7471(73)90041-7

Reyes-Macaya, D., Hoogakker, B., Martínez-Méndez, G., Llanillo, P. J., Grasse, P., Mohtadi, M., Mix, A., Leng, M. J., Struck, U., McCorkle, D. C., Troncoso, M., Gayo, E. M., Lange, C. B., Farias, L., Carhuapoma, W., Graco, M., Cornejo-D'Ottone, M., De Pol Holz, R., Fernandez, C., … Hebbeln, D. (2022). Isotopic Characterization of Water Masses in the Southeast Pacific Region: Paleoceanographic Implications. *Journal of Geophysical Research: Oceans*, *127*(1), e2021JC017525. https://doi.org/10.1029/2021JC017525

Rhines, P. B., & Holland, W. R. (1979). A theoretical discussion of eddy-driven mean flows. *Dynamics of Atmospheres and Oceans*, *3*(2-4), 289-325. https://doi.org/10.1016/0377-0265(79)90015-0

Schulze Chretien, L. M., & Speer, K. (2019). A Deep Eastern Boundary Current in the Chile Basin. *Journal of Geophysical Research: Oceans*, *124*(1), 27-40. https://doi.org/10.1029/2018JC014400

https://doi.org/10.5194/egusphere-2025-1311
Preprint. Discussion started: 31 March 2025

Shaffer, G., Hormazabal, S., Pizarro, O., & Ramos, M. (2004). Circulation and variability in the Chile Basin. *Deep Sea Research Part I: Oceanographic Research Papers*, *51*(10), 1367-1386. https://doi.org/10.1016/j.dsr.2004.05.006

Shaffer, G., Hormazabal, S., Pizarro, O., & Salinas, S. (1999). Seasonal and interannual variability of currents and temperature off central Chile. *Journal of Geophysical Research: Oceans*, *104*(C12), 29951-29961. https://doi.org/10.1029/1999JC900253

Shaffer, G., Pizarro, O., Djurfeldt, L., Salinas, S., & Rutllant, J. (1997). Circulation and Low-Frequency Variability near the Chilean Coast: Remotely Forced Fluctuations during the 1991–92 El Niño. *Journal of Physical Oceanography*, *27*(2), 217-235. https://doi.org/10.1175/1520-0485(1997)027<0217:CALFVN>2.0.CO;2

Stewart, A. L., Wang, Y., Solodoch, A., Chen, R., & McWilliams, J. C. (2024). Formation of Eastern Boundary Undercurrents via Mesoscale Eddy Rectification. *Journal of Physical Oceanography*, *54*(8), 1765-1785. https://doi.org/10.1175/JPO-D-23-0196.1

Stommel, H. (1948). The westward intensification of wind-driven ocean currents. *Eos, Transactions American Geophysical Union*, *29*(2), 202-206. https://doi.org/10.1029/TR029i002p00202

Tsimplis, M. N., Bacon, S., & Bryden, H. L. (1998). The circulation of the subtropical South Pacific derived from hydrographic data. *Journal of Geophysical Research: Oceans*, *103*(C10), 21443-21468. https://doi.org/10.1029/98JC01881

Ulloa, O., Moreno, M., & Pizarro, O. (2023, november 15). Chile completes the installation of its first Integrated Deep-Ocean Observing System. *POGO-Ocean News*. https://pogo-ocean.org/news/chile-completes-the-installation-of-its-first-integrated-deep-ocean-observing-system/

Vega, A., du-Penhoat, Y., Dewitte, B., & Pizarro, O. (2003). Equatorial forcing of interannual Rossby waves in the eastern South Pacific. *Geophysical Research Letters*, *30*(5), 2002GL015886. https://doi.org/10.1029/2002GL015886

Vergara, O., Dewitte, B., Ramos, M., & Pizarro, O. (2017). Vertical energy flux at E NSO time scales in the subthermocline of the S outheastern P acific. *Journal of Geophysical Research: Oceans*, *122*(7), 6011-6038. https://doi.org/10.1002/2016JC012614

Völker, D., Wiedicke, M., Ladage, S., Gaedicke, C., Reichert, C., Rauch, K., Kramer, W., & Heubeck, C. (2006). Latitudinal Variation in Sedimentary Processes in the Peru-Chile Trench off Central Chile. En O. Oncken, G. Chong, G. Franz, P. Giese, H.-J. Götze, V. A. Ramos, M. R. Strecker, & P. Wigger (Eds.), *The Andes* (pp. 193-216). Springer Berlin Heidelberg. https://doi.org/10.1007/978-3-540-48684-8_9

Warren, B. A. (1973). Transpacific hydrographic sections at lats. 43°S and 28°S: The SCORPIO expedition—II. deep water. *Deep Sea Research and Oceanographic Abstracts*, *20*(1), 9-38. https://doi.org/10.1016/0011-7471(73)90040-5

Wijffels, S. E., Toole, J. M., & Davis, R. (2001). Revisiting the South Pacific subtropical circulation: A synthesis of World Ocean Circulation Experiment observations along 32°S. *Journal of Geophysical Research: Oceans*, *106*(C9), 19481-19513. https://doi.org/10.1029/1999JC000118

https://doi.org/10.5194/egusphere-2025-1311
Preprint. Discussion started: 31 March 2025

Wolter, K., & Timlin, M. S. (1998). Measuring the strength of ENSO events: How does 1997/98 rank? *Weather*, *53*(9), 315-324. https://doi.org/10.1002/j.1477-8696.1998.tb06408.x

Yang, X., Tziperman, E., & Speer, K. (2020). Deep Eastern Boundary Currents: Realistic Simulations and Vorticity Budgets. *Journal of Physical Oceanography*, *50*(11), 3077-3094. https://doi.org/10.1175/JPO-D-20-0002.1

Yang, X., Tziperman, E., & Speer, K. (2020). Dynamics of Deep Ocean Eastern Boundary Currents. *Geophysical Research Letters*, *47*(1), e2019GL085396. https://doi.org/10.1029/2019GL085396

Yang, X., Tziperman, E., & Speer, K. (2021). Deep Eastern Boundary Currents: Idealized Models and Dynamics. *Journal of Physical Oceanography*, *51*(4), 989-1005. https://doi.org/10.1175/JPO-D-20-0227.1

Zilberman, N. V., Thierry, V., King, B., Alford, M., André, X., Balem, K., Briggs, N., Chen, Z., Cabanes, C., Coppola, L., Dall'Olmo, G., Desbruyères, D., Fernandez, D., Foppert, A., Gardner, W., Gasparin, F., Hally, B., Hosoda, S., Johnson, G. C., … Van Wijk, E. M. (2023). Observing the full ocean volume using Deep Argo floats. *Frontiers in Marine Science*, *10*, 1287867. https://doi.org/10.3389/fmars.2023.1287867